JCI insight

Elevating EGFR-MAPK program by a non-conventional Cdc42 enhances intestinal epithelial survival and regeneration

Xiao Zhang, Sheila Bandyopadhyay, Leandro P. Araujo, Kevin Tong, Juan Flores, Daniel Laubitz, Yanlin Zhao, George Yap, Jingren Wang, Qingze Zou, Ronaldo P. Ferraris, Lanjing Zhang, Wenwei Hu, Edward M. Bonder, Pawel R. Kiela, Robert J. Coffey, Michael Verzi, Ivaylo I. Ivanov, Nan Gao

JCI Insight. 2020. https://doi.org/10.1172/jci.insight.135923.

Research In-Press Preview **Gastroenterology** **Stem cells**

The regulatory mechanisms enabling the intestinal epithelium to maintain a high degree of regenerative capacity during mucosal injury remain unclear. *Ex vivo* survival and clonogenicity of intestinal stem cells (ISCs) strictly required Cdc42-mediated growth response and Cdc42-deficient enteroids undergo rapid apoptosis. Mechanistically, Cdc42 engaging with EGFR was required for EGF-stimulated receptor-mediated endocytosis and sufficient to promote MAPK signaling. Proteomics and kinase analysis revealed that a physiological, but non-conventionally, spliced Cdc42 variant 2 (V2), exhibited stronger MAPK-activating capability. Human CDC42-V2 is transcriptionally elevated in some colon tumor tissues. Accordingly, mice engineered to overexpress Cdc42-V2 in intestinal epithelium showed elevated MAPK signaling, enhanced regeneration, and reduced mucosal damage in response to irradiation. Overproducing Cdc42-V2 specifically in mouse ISCs enhanced intestinal regeneration following injury. Thus, the intrinsic Cdc42-MAPK program is required for intestinal epithelial regeneration while elevating this signaling cascade is capable of initiating protection from genotoxic injury.

Elevating EGFR-MAPK program by a non-conventional Cdc42 enhances intestinal epithelial survival and regeneration

Xiao Zhang[1], Sheila Bandyopadhyay[1], Leandro Pires Araujo[2], Kevin Tong[3], Juan Flores[1], Daniel Laubitz[4], Yanlin Zhao[5], George Yap[5], Jingren Wang[6], Qingze Zou[6], Ronaldo Ferraris[7], Lanjing Zhang[1,8], Wenwei Hu[9], Edward M. Bonder[1], Pawel Kiela[4], Robert Coffey[10], Michael P. Verzi[3], Ivaylo I. Ivanov[2] & Nan Gao[1,9]*

1. Department of Biological Sciences, Rutgers University, Newark, NJ 07102, USA
2. Department of Microbiology and Immunology, Vagelos College of Physicians and Surgeons, Columbia University, New York, NY 10032, USA
3. Department of Genetics, Rutgers University, New Brunswick, NJ 08854, USA
4. Department of Pediatrics, The University of Arizona, Tucson, AZ 05724, USA
5. Center for Immunity and Inflammation, Rutgers New Jersey Medical School, Newark, NJ 07101
6. Department of Mechanical and Aerospace Engineering, Rutgers University, Piscataway, NJ 08854, USA
7. Department of Pharmacology, Physiology and Neuroscience, Rutgers New Jersey Medical School, Newark, NJ 07101, USA
8. Department of Pathology, University Medical Center of Princeton, Plainsboro, NJ 08540, USA
9. Rutgers Institute of New Jersey, New Brunswick, NJ 08854, USA
10. Department of Medicine/Gastroenterology and Epithelial Biology Center, Vanderbilt University Medical Center, Nashville, TN 37232, USA

Corresponding Author: Nan Gao, Ph.D.

Mailing address: 195 University Avenue, Boyden Hall 206, Newark, NJ 07102

Phone number: 1-973-353-5523

Email: ngao@rutgers.edu

Keywords: CDC42, EGFR, Intestinal Stem Cell, Endocytosis, MAPK.

The authors declare no conflict of interest.

SUMMARY

The regulatory mechanisms enabling the intestinal epithelium to maintain a high degree of regenerative capacity during mucosal injury remain unclear. *Ex vivo* survival and clonogenicity of intestinal stem cells (ISCs) strictly required Cdc42-mediated growth response and Cdc42-deficient enteroids undergo rapid apoptosis. Mechanistically, Cdc42 engaging with EGFR was required for EGF-stimulated receptor-mediated endocytosis and sufficient to promote MAPK signaling. Proteomics and kinase analysis revealed that a physiological, but non-conventionally, spliced Cdc42 variant 2 (V2), exhibited stronger MAPK-activating capability. Human CDC42-V2 is transcriptionally elevated in some colon tumor tissues. Accordingly, mice engineered to overexpress Cdc42-V2 in intestinal epithelium showed elevated MAPK signaling, enhanced regeneration, and reduced mucosal damage in response to irradiation. Overproducing Cdc42-V2 specifically in mouse ISCs enhanced intestinal regeneration following injury. Thus, the intrinsic Cdc42-MAPK program is required for intestinal epithelial regeneration while elevating this signaling cascade is capable of initiating protection from genotoxic injury.

INTRODUCTION

The intestinal epithelia are essential for nutrient absorption and survival of the host. Proper functioning of intestinal epithelial cells (IECs) relies on a signaling network that sustains continued cell production while simultaneously maintaining tissue integrity and retaining the crucial balance among progenitor and differentiated cell populations. Canonical Wnt and EGF signaling are two major growth pathways for intestinal stem cell (ISC) survival and renewal (1-4), while the BMP pathway drives formation of differentiated villus epithelia (5, 6). It is becoming increasingly evident that synergistic interplay of these pathways ensure a homeostasis balance, where crypt-based ISCs self-renew and produce various lineages of progenitors that, upon transit amplification, differentiate into mature IECs to offset programmed cell death (7, 8). Indispensability of Wnt, EGF, and BMP pathways for ISC function are unequivocally demonstrated in enteroid culture system, in which an indefinite ISC renewal is sustained by Wnt and EGF pathway agonists along with BMP pathway inhibitor, Noggin (9-11). Surprisingly, in contrast to enteroid models, intestinal epithelia in animals demonstrate remarkable plasticity displayed by stemness acquisition by quiescent and mature cell populations in response to injury-induced ISC loss (3, 12-21). The interactive complexity of intrinsic and non-intrinsic epithelial signaling that confers remarkable tissue plasticity remains both poorly defined and of important biomedical impact.

The cell division control 42 (Cdc42) is a Rho subfamily small GTPase with pleiotropic functions in cytoskeleton organization, cell polarity, and cell migration across eukaryotic species (22-24). Previously, we reported that elevated Cdc42 levels were observed in human and mouse intestinal tumors (25). Genome wide association study identified a single nucleotide polymorphism in *CDC42* linked to *Irritable Bowel Syndrome* (26). Genetic ablation of *Cdc42* in mouse IECs resulted in enteropathy resembling a lethal form of the pediatric disorder, *Microvillus Inclusion Disease* (27-30). The initial link between Cdc42 and ISC homeostasis was made based on the observation of abnormal organization of intestinal crypts in mice lacking epithelial Cdc42 (28). It remains unclear how Cdc42 controls ISC renewal and regeneration, and whether modulating Cdc42 signaling networks may enhance ISC function.

Using proteomics and kinase assay screening, we identified the involvement of Cdc42 in endocytosis associated EGF-EGFR-MAPK signaling. Elimination of Cdc42 in enteroids resulted in rapid apoptosis, coincident with lost EGF-stimulated EGFR vesicular traffic. We found that native Cdc42 splice variant 2 (V2) (31-36) has enhanced EGFR engagement and MAPK-activating capacity. Mice engineered to produce Cdc42-V2 in intestinal epithelia exhibited robust regenerative

capability and mitigated injury-induced damage. These results shed fresh insight into the role of epithelial intrinsic survival program in mediating protection from stem cell injury.

RESULTS

Cdc42 is indispensable for enteroid survival

Cdc42$_{\Delta IEC}$ mice with constitutive IEC-specific *Cdc42* ablation via *Villin-Cre* were viable (28). However, crypts isolated from *Cdc42$_{\Delta IEC}$* mice did not develop into enteroids in EGF, Noggin, and R-Spondin (ENR)-containing medium. Within 24 hrs after seeding, all *Cdc42$_{\Delta IEC}$* crypts were growth-arrested **(Suppl. Fig. 1A)**. As this growth deficit could be secondary to abnormal development by *Cdc42$_{\Delta IEC}$* intestinal epithelia, we use *Villin-CreER* to delete *Cdc42* from mature *Cdc42$_{Fl/Fl}$; Villin-CreER* (*Cdc42$_{iKO}$*) enteroids. Forty-eight hours after 4-hydroxytamoxifen (4-OHT) addition, the epithelial buds in over 60% of *Cdc42$_{iKO}$* enteroids regressed with cell death and cellular debris **(Fig. 1A, B; Suppl. Fig. 1B)**. After 72 hrs, 95% of *Cdc42-iKO* enteroids accumulated significant amounts of propidium iodide indicative of massive cell death **(Fig. 1B)**, which was further corroborated by elevated numbers of cleaved caspase 3-positive cells **(Fig. 1C)** and a loss of over 90% live enteroid cells quantified by the cell titer-Glo 3D viability assay **(Fig. 1D)**. Viable enteroid were not detected at 5 days after *Cdc42* deletion and the growth of *wild type (WT)* enteroids was not affected by 4-OHT over this time period **(Fig. 1A-D)**. Thus, maintenance of enteroid growth in ENR medium absolutely was dependent upon Cdc42 expression.

Cdc42 is required for and sufficient to promote EGF-MAPK signaling *ex vivo*

We first speculated a disrupted Wnt signaling in Cdc42-deficient enteroids therefore we tried to rescue the growth of by enhancing canonical Wnt signaling via the GSK3-β inhibitor CHIR99021. However, we failed to observe a reversing effect on the death **(Suppl. Fig. 1C)**, suggesting that canonical Wnt pathway was not the primary pathway impacted by Cdc42 deficiency. Treating serum starved human Caco2 cells with EGF ligands (EGF and TGFα), canonical Wnt ligand (Wnt3a), or Noggin activated Cdc42 GTPase activities within minutes **(Suppl. Fig. 1D)**, suggesting that multiple ISC growth factors could act through Cdc42 machinery.

These results led us to conducting an unbiased proteomic search for Cdc42-regulated survival signaling. Parallel mass spectrometry was done on canonical Cdc42 (V1) and its splicing variant (V2), both of which were 3xFlag-tagged and transfected to HEK293 cells. Proteomic analysis of Cdc42 V1- and V2 immunoprecipitates identified an overlapped interactome, where the 5 top

functional clusters mapped to cell cycle, cell division, clathrin-coated endocytosis, mitosis, and MAPK cascade components ($p<0.001$, **Fig. 1E, Suppl. Fig. 1E, F)**.

The identification of a clathrin and MAPK interactome components suggests that Cdc42 may control MAPK activation through clathrin-dependent endocytic EGF receptor signaling (37-41). EGF stimulates rapid receptor-mediated endocytosis that generates changes in plasma membrane elasticity measurable by atomic force microscope (42). Within 30 seconds of EGF loading, there was a robust increase in nanomechanical stiffness on the surface of control Caco2 cells (blue line, **Fig. 1F**). This response was abolished in cells pretreated with the endocytosis inhibitor dynasore (green line, **Fig. 1F**) (43). *Cdc42*-knockdown cells produced a much diminished (89% reduction in stiffness) and a delayed (by 10 mins) response to EGF ligands (pink line, **Fig. 1F**). This impaired nanomechanical response to EGF coincided with reduced intracellular pERK1/2 levels in *Cdc42*-knockdown cells **(Fig. 1G)**, illustrating Cdc42's requirement for EGF-stimulated endocytosis.

To further dissect signaling cascades downstream of Cdc42, we examined 43 major intracellular kinase targets in HEK293 cells overexpressing either Cdc42 V1 or V2. Compared with cells expressing empty vector, phosphorylation levels of 3 major MAPK components, ERK1/2, c-Jun, and p38, were elevated in Cdc42-overexpressing cells, especially in V2-overexpressing cells **(Fig. 1H**, **and Suppl. Fig. 1G)**. We validated this finding in a time course experiment, in which overexpressing Cdc42 resulted in a 5-fold increase in pERK1/2 (V2 shown in **Fig. 1I**). In addition to EGFs, canonical Wnt has also been shown to trans-activate ERK (44). In the presence of Wnt3a, an ISC growth factor, Cdc42-V2 robustly elevated pERK1/2 (**Fig. 1I, J**). A side-by-side comparison of ERK-activating capabilities of the two variants showed that V2's strength was 230% of V1 **(Fig. 1J)**.

The stronger MAPK-activating capabilities by V2 were not due to different binding to the Cdc42 effector PAK1, which equally associated to both variants **(Suppl. Fig. 1H)**. Cdc42 V1 and V2 differ in the last 10 amino acids. Mutation of V2-specific lysine 185 (K185R) within the C-terminus poly-lysine region reported to be essential for membrane attachment (45-47), led to a markedly reduction in pERK1/2 levels **(Fig. 1K)**, suggesting that Cdc42's MAPK-stimulating activity requires membrane association.

Cdc42 is required for EGF receptor endocytosis

To examine the intrinsic impact of loss of Cdc42 on EGFR endocytic signalosome in the intestinal epithelium, *Cdc42* was inducibly knocked-out in mature Cdc42$_{iKO}$ enteroids. Forty-eight hrs following 4-OHT treatment, Cdc42$_{iKO}$ enteroid cells showed a noticeable loss of polarized intracellular EGFR distribution **(Fig. 2A, B)** and a reduction in pHH3$_{+}$ mitotic activity **(Fig. 2A, C)**. We performed a time-

course experiment to determine whether EGFR delocalization preceded enteroid cell death. Twenty-four hrs after 4-OHT addition, 45% of enteroid cells exhibited altered localization of EGFR **(Fig. 2D, E)**, while apoptotic cells remained rare **(**below 5%, **Suppl. Fig. 2A, B)**. At 40 hr, approximately 80% of enteroid cells showed EGFR delocalization, but the vast majority of apoptotic events only occurred after 40 hr and peaked at 72 hr **(Suppl. Fig. 2A, B)**. These data suggested that EGFR abnormality occurred prior to enteroid cell death, suggesting a possible link between EGFR abnormality and survival.

To directly observe EGFR trafficking *in vivo*, Cdc42iKO mice were crossed to a CRISPR-CAS9 engineered emerald-EGFR (emEGFR) mouse allele (48). Administration of a pulse of EGF to WT mice elicited a marked induction, within 30 min, of emEGFR vesicles as well as emEGFR$_+$/early endosome antigen (EEA)$_+$ vesicles **(Fig. 2F, G)**, which were diminished in Cdc42$_{iKO}$ crypt cells **(Fig. 2H).** This reduction of EGF-stimulated endocytic "signalosomes" in Cdc42$_{iKO}$ crypt cells echoed significant decreases in levels of pErbB1(Y1068) and pErbB2 (Y1221/1222), active forms of major EGF receptors in Cdc42$_{iKO}$ IECs **(Fig. 2I, J)**. Of note, total levels of both receptors were increased and there were residual pErbB1, pErbB2, pErk1/2 in Cdc42$_{iKO}$ IECs **(Fig. 2I, J)**. These data suggested a changed EGFR compartmentalization and a possibly affected MAPK activation in Cdc42$_{iKO}$ IECs *in vivo*.

Cdc42 engages EGFR and endocytosis machinery

Ligand-stimulated EGF receptors are associated with lipid rafts that are internalized to transduce MAPK signaling (49-53). When lipid rafts were extracted from V2-overexpressing cells using Optiprep gradient cellular fractionation (54), a pool of V2 co-sedimented with the lipid raft proteins Flotillin (55) and Caveolin-1 (56) along with, EGFR, tyrosine receptor Fyn (57), Phosphoinositide 3-kinases (PI3K) (58), and Wnt-activated pLrp6 (59, 60) **(Fig. 3A)**.

Co-immunoprecipitation (co-IP) analysis indicated that both V1 and V2 associated with EGFR through binding to the receptor's intracellular domain (ICD) **(Fig. 3B,** see IP Flag panel) and this was further validated for endogenous EGFR and Cdc42 variants **(Fig. 3C)**. Compared to Cdc42 V1, the V2-variant exhibited a stronger association towards both EGFR and clathrin **(Fig. 3C)**, consistent with V2's demonstrated stronger MAPK-activating capability **(Fig. 1J)**. A further examination of Cdc42 interactomes identified numerous structural and signaling components, including actin, IQGAP1/2/3, clathrin, AP-2, Arp2/3, MAPKKK7, p38, PAK4, etc. **(Suppl. Table 1; Suppl. Fig 2C)** reported to be involved in EGFR endocytosis and MAPK cascade (61-65)**(Fig. 3D).** Thus, Cdc42 directly engaged EGFR endocytosis machinery for MAPK signaling.

IEC overexpression of Cdc42-V2 altered epithelial differentiation program

To date, study of Cdc42 has been hampered by the absence of a specific gain-of-function *in vivo* model. We found that, in contrast to the ubiquitous expression of Cdc42 V1, expression of V2 could be detected in mouse enteroids **(Suppl. Fig. 3A)** and fetal intestines, while its level was reduced in adult intestines **(Suppl. Fig. 3B)**. Based on V2's stronger MAPK-activating capacity, we sought to determine if elevating Cdc42 activity in adult IECs by overexpressing the variant 2 (V2, a naturally expressed protein) might enhance epithelial survival *in vivo*. We thus established an inducible mouse allele (referred to as $V2_{Tg}$), which allowed a Cre-activated cell-specific production of a Flag-tagged Cdc42-V2 **(Fig. 4A)**.

We validated IEC-specific Cdc42-V2 production in small intestinal and colonic epithelia of independent $V2_{Tg}$ founders crossed to *Villin-Cre* or *Villin-CreER* drivers by western blot **(Fig. 4B)** and by immunohistochemistry **(Fig. 4C)**. A $V2_{Tg}$ founder producing V2 at approximately 40% of endogenous Cdc42 was selected for further experiments **(Fig. 4D)**. *Villin-Cre;*$V2_{Tg}$ intestines had longer villi and more crypts **(Fig. 4E, Suppl. Fig. 4A, B)**. Examination of intestinal epithelial cell types revealed that $V2_{Tg}$ intestine had a reduction of Tuft cells by 80% **(Fig. 4G, Suppl. Fig. 4C-E)** but had no change in goblet cells **(Fig. 4F, H).** In contrast, *Cdc42*$_{\Delta IEC}$ intestines showed a complete loss of Tuft cells and an 30% increase in goblet cells **(Fig. 4G, Suppl. Fig. 4C-E)**.

Interestingly, expressing *V2*$_{Tg}$ in *Cdc42*$_{\Delta IEC}$ intestinal epithelium significantly mitigated the Paneth cell defect **(Fig. 4I, K)** and microvillus inclusion phenotype **(Fig. 4J, L, Suppl. Fig. 4F)** previously reported in *Cdc42*$_{\Delta IEC}$ intestines (28). These data functionally validated this newly developed *V2*$_{Tg}$ mouse allele and revealed an unknown impact of Cdc42 on Tuft cell differentiation.

Overexpressing Cdc42-V2 robustly elevated ISC function *in vivo*

Inhibition of MAPK by EGFR inhibitor in enteroid culture was shown to promote Tuft cell differentiation (3). The observed loss of Tuft cell differentiation in both gain- and loss-of-Cdc42 function prompted us to examine the impact of Cdc42 on MAPK activity and ISC function. Quantitative RT-PCR detected a 5-fold increase in *Cdc42* mRNA level in ISC-enriched enteroids treated with CHIR99021 and valproic acid (66, 67) as compared to enteroids typically grown in ENR medium **(Fig. 5A)**. Bulk RNA-seq of *Cdc42*$_{\Delta IEC}$ intestines affirmed a transcriptomic reduction of Lgr5 ISC gene signature (p=0.007, **Fig. 5B**).

Cdc42$_{\Delta IEC}$ mice had shorter intestines (73% of WT littermates, **Fig. 5C, D**), while *Villin-Cre;V2$_{Tg}$* mice with elevated Cdc42-V2 in IECs had longer intestines, 112% of WT mice **(Fig. 5C, D)**, indicative of enhanced ISC function (68, 69). *V2$_{Tg}$* intestines had increased Olfm4 levels in crypts **(Fig. 5E, F)**, and elevated gene signatures of both fast-cycling and "quiescent" ISCs, in particular Bmi1 **(Suppl. Fig. 5A)**. Importantly, a pronounced expansion of pErk1/2$_+$ active cell population to the villus region was detected in *V2$_{Tg}$* intestines **(Fig. 5G, H)**. By contrast, pErk1/2$_+$ cells in WT mice were restricted to crypt and transit amplifying compartments as previously reported (70, 71). Scattered pErk1/2$_+$ cells were present throughout *Cdc42$_{\Delta IEC}$* villus epithelium. We also detected an elevated beta-catenin levels in *V2$_{Tg}$* intestines **(Suppl. Fig. 5B, C)**, in overall agreement with an enhanced ISC function in homeostasis.

We established *Cdc42$_{\Delta IEC}$; V2$_{Tg}$* mice where deletion of endogenous Cdc42 and production of the V2 transgene were driven by Cre in same IECs. *Cdc42$_{\Delta IEC}$*; V2$_{Tg}$ mice showed largely restored IEC phenotypes compared to *Cdc42$_{\Delta IEC}$* mice **(Fig. 5C-H)**. These phenotypic restorations were accompanied by restoration of pErbB1, pErbB2, and pErk1/2 levels in *Cdc42$_{\Delta IEC}$*; V2$_{Tg}$ mouse intestines **(Fig. 2I)**. Ex vivo, V2$_{Tg}$ enteroids exhibited a much more robust epithelial budding **(Fig. 5I, K)**, larger sizes **(Fig. 5J, K)**, and increased proliferation activities **(Fig. 5L)**. Thus, elevating epithelial Cdc42-V2 autonomously enhanced ISC function at steady state.

Cdc42-V2 mitigates injury-induced epithelial damage

Prompted by above results, the impact of V2 expression on epithelial regeneration after injury was examined. ISCs are sensitive to irradiation (72) with fast-cycling ISCs dying within 2 days after irradiation (73-75). Mice were exposed to 12 Gy total-body irradiation **(Fig.6A).** Compared to WT littermates, Cdc42$_{\Delta IEC}$ mice lost nearly 25% of body weight 4 days after irradiation **(**green line, **Fig. 6B)**. This was accompanied by declining body conditions and 25% post-irradiation mortality of Cdc42$_{\Delta IEC}$ mice within a week. All *WT*, *V2$_{Tg}$*, and *Cdc42$_{\Delta IEC}$; V2$_{Tg}$* mice survived the experimental duration. *V2$_{Tg}$* mice were resistant to body weight loss and exhibited an earlier weight recovery **(**red line, **Fig. 6B)**, while *Cdc42$_{\Delta IEC}$; V2$_{Tg}$* mice showed improved body weight and health condition compared to *Cdc42$_{\Delta IEC}$* mice **(**purple line, **Fig. 6B)**. Examination of intestines revealed that *Cdc42$_{\Delta IEC}$* intestines were 24% shorter than WTs **(Suppl. Fig. 6A-B)**, with reduced numbers of regenerative crypts **(Fig. 6C, D, Suppl. Fig. 6C)**. Consistent with the elevation of stem cell marker mRNA level, more Olfm4$_+$ cells were detected in each crypt of the V2$_{Tg}$ mice **(Fig. 6E, F).** Likewise, there were overall more Olfm4$_+$ crypts in V2$_{Tg}$ mice than in WT mice **(Suppl. Fig. 6D, E)**. Furthermore, 24-hr

EdU labeling (red) followed by a 30-min BrdU labeling (green) before sacrifice **(Fig. 6A)** indicated that *Cdc42$_{\Delta IEC}$* mice had reduced cycling cells as well as cell-cycle re-entry indicated by EdU^{+}/BrdU^{+} cells **(Fig. 6G, H).** *Cdc42$_{\Delta IEC}$* mice also had reduced numbers of cells migrating into villus epithelia **(**arrows in **Fig. 6H, I)**. Cdc42 V2 overexpression enhanced IEC proliferation and migration and restored above-illustrated phenotypic defects in *Cdc42$_{\Delta IEC}$; V2$_{Tg}$* mice **(Fig. 6B-I, Suppl. Fig. 6A-E).**

Overexpressing Cdc42 V2 in ISCs enhanced epithelial lineage tracing after irradiation injury.

qPCR showed significantly elevated expression of canonical CDC42 (V1) in human colorectal cancer tissues, compared to adjacent normal tissues **(**N=41 pairs of samples; **Fig. 7A),** consistent with a previous report (76). Using a CDC42 V2 specific Taqman probe, we detected an average of 2.5-fold increase in cancer tissues compared to adjacent normal tissues **(**N=28 pairs of samples; **Fig. 7A)**. In addition, Lgr5^{EGFP+} ISCs FACS-sorted from wild type Lgr5$^{CreER\text{-}IRES\text{-}EGFP}$ mouse duodenum and ileum showed elevated expression levels of both Cdc42 variants when compared to sorted Lgr5^{EGFP-} epithelial cells **(Fig. 7B, C).** We concluded that although Cdc42 is ubiquitously expressed in all epithelial cells, both variants are preferentially elevated in proliferating cells.

As compared to WT mice, *V2$_{Tg}$* mice exhibited a resistance to irradiation-induced loss of Olfm4+ cells **(Fig. 6G-I),** this suggested that a higher level of Cdc42 V2 might favor ISC survival and regeneration. Pan-IEC Cre drivers, such as Villin-Cre, shed limited insights to the role of Cdc42 specific to ISCs, we specifically overexpressed V2$_{Tg}$ in Lgr5 ISCs by deriving *Lgr5$^{CreER\text{-}IRES\text{-}EGFP}$; R26R^{zsGreen}; V2$_{Tg}$* mice. Lineage-tracing of Lgr5^{+} ISCs was conducted 3 days after 12 Gy irradiation of *Lgr5$^{CreER\text{-}IRES\text{-}EGFP}$; R26R^{zsGreen}; V2$_{Tg}$* mice, where V2 overproduction was initiated from Lgr5 ISCs. Compared to Cdc42-WT mice, *Lgr5$^{CreER\text{-}IRES\text{-}EGFP}$; R26R^{zsGreen}; V2$_{Tg}$* mice showed significantly more lineage tracing events **(**illustrated by ratio of green stripes / green crypts, **Fig. 7D, E)**, which were accompanied by elevated mitotic cells in traced crypts **(Fig. 7F, G)**. Nonetheless, ISCs overexpressing V2$_{Tg}$ did not appear to have elevated levels of nuclear β-catenin **(Fig. 7H, I)**, again suggesting that the enhanced epithelial regeneration was not directly related to canonical Wnt signaling.

In contrast, *Cdc42$_{Fl/FL}$; Lgr5$^{CreER\text{-}IRES\text{-}EGFP}$; R26R^{zsGreen}* mice lacking Cdc42 in ISCs showed drastically reduced lineage tracing events after irradiation **(Fig. 7D, E)** accompanied by a reduced mitosis **(Fig. 7F, G).** Taken together, our data suggested that Cdc42 is an epithelial intrinsic machinery essential for mucosal repair in response to injury-induced damage.

DISCUSSION

This report provides molecular, genetic, and cell biological insight into the underlying mechanism of the extraordinary regenerative capacity of intestinal epithelium in response to injury. Our data shed lights on how exactly Cdc42 potentiates MAPK pathway and possibly other signaling pathways related to ISC survival. Based on atomic force microscopic study, proteomics, and kinase array analysis, we showed that Cdc42 is required for ligand-stimulated EGFR endocytosis and MAPK signaling. Cdc42-deficient IECs lost responses to both EGF and Wnt ligands that activate MAPK.

Rho family GTPases (Rho, Cdc42 and Rac) share a set of GEF, GAP, GDI, and downstream effector proteins, and are involved in regulating common signaling transduction pathways (77) (78) (79). Cdc42 sometimes exhibits distinct functions from the other two Rho GTPase members (80) (81). Notably, Cdc42 inhibited activities of Rho, for example, in the regulation of epithelial cell apical tension (82) or during activation of Rhotekin in optic tectal cells (83). Regarding EGFR/MAPK signaling, *in vitro* studies showed that Rac was activated by EGF during colonic epithelial migration (84) and during MAPK mediated Cox2 production (85). Thus, Rac might be playing a role downstream of EGF-MAPK cascade in the intestinal epithelium. This might partially explain the fact there was no compensatory mechanism ex vivo to rescue the death of Cdc42-deficient enteroids.

Multiple gain- and loss-of-function experimental platforms in our study consistently supported an impact of Cdc42 on EGFR-MAPK pathway. EGFR signaling possesses a foundationally conserved role in regulating gut development and cell proliferation in lower (86-92) and higher eukaryotic species (93, 94). The requirement of EGF initiated signaling for epithelial survival and renewal is extensively documented (48, 95-98), and is proposed to keep $Lgr5_+$ ISCs in a constitutively active state (3). EGFR-MAPK signaling may enhance intestinal epithelial survival by preventing cell shedding (99). Proper intraepithelial EGFR localization has also been shown to define cell-type specific functions (100). These studies and the reported contribution of EGFR signaling to injury-induced tissue regeneration (101, 102) were consistent with our observed impact of Cdc42 on EGFR-MAPK cascade and cell survival *in vitro* and *in vivo*.

Within the lipid raft compartment, Cdc42 was also co-sedimented with Wnt receptor and PI3K. Thus. Cdc42 must also cross talk with other signaling components that utilize endocytic machinery, such as the Wnt and PI3K cascades. Cdc42 loss- or gain-of-function was likely to exert pleiotropic influences on other non-EGF survival pathways. Nevertheless, our data revealed a more consistent impact of Cdc42 on MAPK signaling than its impact on other pathways. Both Wnt and EGF are ISC niche factors, and both had been documented to activate MAPK pathway (103). For example, Wnt3a activates JNK (104), p38 (62), and ERK (105). Wnt3a could either directly activate ERK via Raf or

through AP1 and TCF (105). Future studies will be necessary to delineate the collateral effects of Cdc42 on each individual signaling pathway.

Although our analysis heavily focused on cell survival signaling, given Cdc42's documented roles in controlling cell polarity and cytoskeletal organization, it is certain that the general Cdc42-dependent structural regulations are closely associated with cellular responses to external growth signals. Cdc42 could control apical and basolateral deployment of membrane proteins, such as EGFR, to facility signal receiving. Cdc42 may also control epithelial junctional integrity thereby impacting Hippo signaling. Furthermore, the observed Paneth cell defects suggested an impact of Cdc42 on the Ephrin-EphB3 signaling shown to regulate Paneth cell positioning at crypts (106). Finally, the formation of microvillus inclusion in Cdc42-deficient enterocytes reflected a robust dysregulation of cortical actin in these cells. Thus, Cdc42-dependent cellular structural regulation must be strongly coupled to its impact on intracellular survival signaling activities.

Cdc42 has 2 physiologically transcribed isoforms with one being universally expressed (V1) while the other (V2) was initially found to be enriched in neuronal tissues. The major distinction between them was a selective splicing into a distinct last exon that encodes for the very C-terminal 10 amino acids. While both variants can be prenylated, only V2 can be palmitoylated at a unique C-terminal cysteine residue that was absent from the conventional Cdc42 (V1)(33). Studies in neuronal cells had suggested Cdc42-V2's stronger incorporation into lipid rafts (32, 33, 35, 107-109), which was proposed as a potential mechanism for its greater traffic and concentration in the dendritic spines (32, 34). It was postulated that Cdc42-V2 acted to promote the formation of subcellular post-synaptic structures, leading to a greater synaptic plasticity during brain activity (35), whereas the canonical Cdc42 aided axonogenesis (31, 36). Our data suggested that the stronger MAPK-activating capability by Cdc42-V2 was likely mediated by its enhanced affiliation with lipid compartments.

The newly engineered Cdc42 $V2_{Tg}$ mice allowed a direct demonstration of a robust impact of Cdc42 gain-of-function on MAPK activation and ISC regeneration. Cdc42-V2 is physiologically expressed in enteroids and intestinal epithelium at lower levels compared to canonical Cdc42. Cdc42 $V2_{Tg}$ mice provided a tool to enhance Cdc42 function. Findings reported here might represent the first step towards the possibility of enhancing ISC function by elevating Cdc42 activity, potentially through promoting the alternative splicing of Cdc42 variant 2 via regulators that had been reported (110). Our observed alterations in intestinal epithelial differentiation in Cdc42 loss- and gain-of-function models added to the reported impact of MAPK on the differentiation of intestinal epithelial cell types, including Paneth cells, goblet cells, and Tuft cells (3, 111, 112). Taken together, the cell-

autonomous effects of Cdc42-V2 on epithelial regeneration have important implication for mitigating gastrointestinal pathologies that require an enhanced tissue repair program.

METHODS

Mice

The Cdc42 flox (113), emEGFR (48), Villin-Cre (114), Villin-CreER (115), Lgr5$_{EGFP\text{-}IRES\text{-}CreER}$ (116), and Rosa26R-ZsGreen mice (117) have been previously described. A conditional *Cdc42-V2$_{Tg}$* mouse allele was established by inserting the 3×Flag-Cdc42-V2 coding sequence downstream of a chick actin (CAG) promoter and a lox-CAT-lox cassette, at the unique BamH1 restriction site, followed by a 225 bp bovine growth hormone poly-A sequence that does not contain coding sequence. All mice were maintained on a 12-hour light/dark cycle and provided with food and water ad libitum in individually ventilated cages under specific-pathogen-free (SPF) conditions at Rutgers University-Newark animal facility. Experimental comparisons were strictly made among littermates.

Total-body γ irradiation

Animals were subjected to total body irradiation using a Caesium-137 irradiator calibrated to a dose of 12 Gy. All procedures follow the biosafety guidelines of Rutgers-New Jersey Medical School.

Tamoxifen administration

Forty mg/kg body weight of tamoxifen in corn oil was injected to mice of 8-12 weeks of age intraperitoneally determined by the experimental scheme. Depending on the experiments, 4-7 days after tamoxifen administration, intestinal tissues were collected for analysis (118). For linage trancing after irradiation, a single dose of tamoxifen was administrated to mice 3 days after irradiation to trace green strip formation by Lgr5 cells that were either Cdc42 deficient or V2-overexpressing. These mice were sacrificed 7 days after irradiation for the analysis of linage tracing and mitotic events.

Administration of EGF to mice

Recombinant mEGF (315-09 B, Peprotech) was injected intraperitoneally at a concentration of 1 μg per gram body weight, 30 minutes prior to tissue collection.

EdU and BrdU incorporation in mice

Mice were intraperitoneally injected with BrdU labeling reagent (00-0103, Invitrogen) at 10 μl/g body weight 30 mins before tissue collection. EdU was injected intraperitoneally into mice at 100 mg/kg for 2, 6 or 24 hrs before tissue collection. Intestinal tissue was embedded in either paraffin or OTC for sectioning. BrdU was detected by BrdU antibody and secondary fluorescent anti-Rat antibody. EdU was detected by a Click-iT EdU Imaging Kit (C10338, Invitrogen).

Immunofluorescence and immunohistochemistry

Intestinal tissues were collected and fixed in 4% paraformaldehyde or 10% neutral formalin buffer and embedded in paraffin. 5 μm sections were sliced, dewaxed, and subjected to antigen retrieval (0.1 M citric acid, pH 6.0 for most of the antibodies except phospho-Stat3 using DAKO Target Retrieval Solution and Signal Stain EDTA Unmasking Solution respectively). Slides were immersed

into antigen retrieval buffer at a sub-boiling temperature for 15 minutes. After incubation with 3% H_2O_2 in methanol for 10 minutes, sections were then blocked in PBS containing 0.1% Triton-X100, 2% BSA and 2% normal serum for at least one hour at room temperature, and then probed with indicated antibodies at 4 °C overnight. Next morning, slides were washed in PBS three times and probed with biotinylated secondary antibody (for IHC) or fluorescence-conjugated secondary antibodies (for immunofluorescence). After one-hour incubation at room temperature, slides were washed three times. For IHC, slides were incubated with streptavidin-conjugated horseradish peroxidase (HRP) for an hour at room temperature. DAB HRP substrate kit was used for development. For immunofluorescence, slides were washed with PBS three times and subsequently subjected to DAPI counter-staining, before being air-dried and mounted with Prolong Gold antifade medium. Immunofluorescent images were collected by LSM 510 Laser Scanning Microscope and analyzed by AIM software (version 4.2) or Fiji software (https://fiji.sc).

Enteroid culture, 4-OH-Tamoxifen treatment *ex vivo*, propidium iodide staining, and cell titer-Glo 3D cell viability assay

Enteroid cultures from Cdc42-deficient or Cdc42-WT mice were conducted based on previously described method (119). To induce Cdc42 deletion in iKO enteroids, 100-200 wild type or Cdc42-iKO crypts were seeded in Matrigel with ENR media and allowed to develop for 3 days. On day 4, 500 nM 4-OHT was added to the enteroids for 24 hrs. Viable enteroids were counted under a bright field microscope 1-7 days after 4-OHT treatment. For propidium iodide staining, enteroids were incubated with 500 nM propidium iodide (P4170, Sigma) in PBS solution at 37°C for 10 min, and washed with PBS before imaging. For 3D cell viability assay, 100 organoids were seeded in each well on a 96 well-plate and cultured in ENR media for 4 days before addition of 4-OHT. Cell viability was determined typically at 72 hrs after 4-OHT treatment using the Cell Titer-Glo 3D Cell Viability Assay (G9681, Promega) by Glomax system (E9032, Promega).

Embedding enteroids for histological analysis

To dissolve Matrigel containing enteroids, medium was removed from wells and treated with 500 µl of Corning Recovery Solution (354253, Corning) on ice for 10 minutes. A p1000 pipette was then used to dissolve remaining Matrigel. Two to three wells of enteroids were combined in a microcentrifuge tube and centrifuged at 200 × g for 5 minutes. Ice cold PBS was used to wash the pellet. After a 2-minute centrifugation at 200 × g, PBS was removed, and enteroids were resuspended in 4% paraformaldehyde for 10-15 minutes. After fixation, enteroids were centrifuged at 200 × g for 5 minutes and washed 3 times in cold PBS. After removing the last PBS wash, 10-20 µl of Matrigel was added to form clump of enteroids and left at 37°C to solidify. Once solid, 70% ethanol was added and stored at 4°C until paraffin embedding at the Histology Core of Rutgers New Jersey Medical School.

CDC42 GLISA assay

Caco2 cells were serum starved overnight and then treated with EGF (50 ng/ml, #315-09 B, Peprotech), Wnt3a (100 ng/ml, #315-20, Peprotech), TGFα (50 ng/ml, #T7924, Sigma), Noggin (100 ng/ml, #250-38, Peprotech), and R-Spondin (1 µg/ml, #3474-RS-050, R&D Systems), respectively.

CDC42 activity was determined before and after treatment by CDC42-specific GLISA assay (#BK127, Cytoskeleton) performed according to the manufacturer's instructions.

Lentivirus-mediated Cdc42 knockdown

To stably knockdown Cdc42 in Caco2 cells, human CDC42-specific lentiviral transduction particles (#TRCN0000047628, Sigma-Aldrich) was added to cells at 1/5 multiplicity of infection with 8 μg/ml Polybrene. Cells infected by non-Target shRNA Control Transduction Particles (#SHC203V, Sigma-Aldrich) were used as control. Infected cells were selected by 10 μg/ml puromycin for 2 weeks. To induce MAPK activation, 100 ng/ml human EGF or 100 ng/ml mouse recombinant Wnt3a was added to serum starved cells for indicated time before cells were harvested for pERK detection.

Transfection of HEK293 cells

HEK293 cells were prepared to reach 70–90% confluent at the time of transfection. 2 μg plasmid DNA was transfected using Lipofectamin 3000 (#L3000008, Invitrogen). Forty-eight hours after transfection, cell lysate was made for further experiments.

Atomic force microscope analysis

A commercial atomic force microscope system (Dimension ICON, by Bruker-Nano Inc., Santa Barbara, CA) was used to measure all the cellular surface plasma membrane properties. As previously published (42), a MLCT-C cantilever was used to measure the Young's modulus of cells, with a spring constant at 0.01 N/m calibrated via the thermal tune method (Bruker-Nano Inc.). To avoid the substrate effect and keep consistency of the measurement conditions, all of the measurements were performed at the top of the cell over the cell nucleus. The probe radius was calibrated by using a tip-radius calibration sample, and a silicon sample was used as the hard reference sample for all the indentation measurements. To minimize the cantilever drift due to the temperature fluctuation caused by the heating of the laser, the system was thermally equilibrated at 37°C for 40 min before the measurements.

Proteomic analysis with mass spectrometry

HEK293T cells were transfected with empty pQCXIP-3×Flag vector, pQCXIP-3×Flag-Cdc42-V1 or pQCXIP-3×Flag-Cdc42-V2. Cell lysates were subjected to immunoprecipitation using a Flag antibody (FLAGIPT1, Sigma-Aldrich). Immunoprecipitates were resolved by NuPAGE™ 4-12% Bis-Tris Protein Gels (NP0335, Thermo Scientific), fixed for 1 hour with fixative containing 50% methanol and 10% acetic acid. After staining with Ruby Red, protein bands were cut for mass spectrometry analysis at Center for Advanced Proteomics Research of Rutgers University. Data was analyzed with Scaffold 4 software, DAVID Bioinformatics Resources 6.8, Excel 3D Scatter Plot v2.1, and esyN (120)

Phospho-kinase array analysis

Lysates from HEK293T cells transfected with empty vector, Cdc42-V1 or Cdc42-V2 were subjected to a kinase array analysis using the Proteome Profiler Human Phospho-Kinase Array (#ARY003B, R&D Systems) according to the manufacturer's instructions.

Optiprep gradient cellular fractionation

HEK293T cells were lysed with buffer composed of 150 mM NaCl, 50 mM Tris-HCl pH 8.0, 5 mM EDTA and 0.5% Triton-X100, supplemented with protease and phosphatase inhibitors. After solubilization for 20 min at 4°C, 300 µl of lysates were combined with 600 µl of 60% Optiprep solution to yield a 900 µl 40% Optiprep-Lysate mixture. After loading this mixture to the bottom of a Beckman ultracentrifuge tube, 3 ml of 30% Optiprep solution (in lysis buffer) and 750 µl of 15% Optiprep solution was overlaid sequentially, followed by 500 µl of pure lysis buffer on the top. Samples were centrifuged at 50,000 rpm for 3.5 hrs in rotor SW41Ti at 4°C. After taking two 800 µl fractions from the top, seven 0.5 ml fractions were collected until the bottom of the tube, used for western blot. Lysates collected at the interface of 15% and 30% were referred to as detergent-resistant fraction (or lipid raft). The rest of fractions were referred to as detergent soluble.

Realtime PCR

Total mRNAs were extracted using QIAGEN RNeasy mini Kit from scraped epithelia. cDNA synthesis was performed using Thermo Scientific Maxima H Minus First Strand cDNA Synthesis Kit. Real-Time PCR reactions were assembled using the SYBR Green Real-Time PCR Master Mixes (Thermo Fisher). Reactions were run in replicates by a Roche Light cycler 480. The PCR cycling conditions were 10 min pre-heating at 95°C followed by 45 cycles of denaturing (95°C for 10 s), annealing (60°C for 10 s) and extension (72°C for 10 s). Fluorescent signal was acquired during the extension phase. Melting curves were analyzed to ensure PCR specificities. House-keeping genes (such as HPRT) were used as internal references. For detection of V1 or V2 specific CDC42 mRNA levels in human colorectal cancers, specific Taqman probes (ID: Hs03044122_g1 for V1; ID: Hs00741586_mH for V2) were used in Taqman quantitative PCR on RNAs of paired human colorectal tumor and adjacent normal tissues.

Bulk RNA-sequencing and gene set enrichment analysis (GSEA)

RNA seq data was deposited at NCBI BioProject with access number GSE124848. GSEA (121, 122), pre-ranked files of differentially expressed genes calculated by the rank metric = -log (p-value) * SIGN (logFC) (123). GSEA was performed on intestinal stem cell gene signatures (124). Normalized enrichment scores (NES) and p-values were documented (K-S Test). Heatmaps of select EGF receptor and cytokine genes were generated by plotting z-scores of fpkm normalized RNA-Seq data of individual replicates.

QUANTIFICATION AND STATISTICAL ANALYSES

Statistical and graphic data analysis was conducted using Prism GraphPad 7.04 (https://www.graphpad.com) and Microsoft Excel 2016. The data were presented as mean ± S.E.M. in bar graphs or in box-whiskers plots. The histology and immunostaining results were reported from 3 to 20 sections of at least 3 mice in each experiment unless stated differently. Each experiment had technical replicates that were reported in graphs to demonstrate intra-sample variations. To quantify immunostaining results, Image J (1.6.0_24 version) IHC toolbox package (https://imagej.nih.gov/ij/plugins/ihc-toolbox/index.html), was used to determine signals within a crypt

or a crypt-villus unit depending on the specific antigen and experiment elaborated in figure legends. At least 20 crypt or villus units were analyzed from each section. Animal numbers used in each experiment were detailed in figure legend. Two-tailed paired student t-test was used for experiments containing two groups unless specifically addressed. A p-value less than 0.05 was considered significant in these t-tests. For animal experiments with more than two groups, One-Way ANOVA and multiple comparison were made, where Bonferroni correction was applied to justify the significance. As a result, in Fig. 4G-H, K-L, Fig. 7E, G, p-value <0.025 was considered significant, and for Fig. 5D, F-G, I-J, Fig. 6B-C, E, G and I, p-value < 0.0167 was considered significant.

STUDY APPROVAL

Experimental procedures in this study were approved by the Institutional Animal Care and Use Committee of Rutgers University**.**

ACKNOWLEDGEMENT:

We thank the Facility of Genome Editing of Rutgers Cancer Institute of New Jersey (P30CA072720) for developing Cdc42 V2Tg mice. This work was supported by: NIH (R21CA178599, R01DK102934, R01AT010243, R01DK119198), ACS Scholar Award (RSG-15-060-01-TBE), NSF/BIO/IDBR (1353890, 1952823), and a Rutgers IMRT award to N.G.; NIH/NCI R01CA190558 to M.P.V.; NSF Grant (IOS- 1456673, IOS-1754783) to R.P.F.; an NIH F31 DK121428-01 to S.B.; NJCCR fellowships (DHFS16PPC036, DHFS17PPC036, DCHS19PPC038) to K.T., S.B., J.F., respectively.

References cited:

1. Krausova M, and Korinek V. Wnt signaling in adult intestinal stem cells and cancer. *Cellular Signalling.* 2014;26(3):570-9.
2. Schepers A, and Clevers H. Wnt Signaling, Stem Cells, and Cancer of the Gastrointestinal Tract. 2012;4(4).
3. Basak O, Beumer J, Wiebrands K, Seno H, van Oudenaarden A, and Clevers H. Induced Quiescence of Lgr5+ Stem Cells in Intestinal Organoids Enables Differentiation of Hormone-Producing Enteroendocrine Cells. *Cell Stem Cell.* 2017;20(2):177-90 e4.
4. Gregorieff A, and Clevers H. Wnt signaling in the intestinal epithelium: from endoderm to cancer. 2005;19(8):877-90.
5. Qi Z, Li Y, Zhao B, Xu C, Liu Y, Li H, et al. BMP restricts stemness of intestinal Lgr5+ stem cells by directly suppressing their signature genes. *Nature communications.* 2017;8:13824.
6. He XC, Zhang J, Tong W-G, Tawfik O, Ross J, Scoville DH, et al. BMP signaling inhibits intestinal stem cell self-renewal through suppression of Wnt–β-catenin signaling. *Nature Genetics.* 2004;36:1117.
7. Clevers H. The Intestinal Crypt, A Prototype Stem Cell Compartment. *Cell.* 2013;154(2):274-84.
8. Gehart H, and Clevers H. Tales from the crypt: new insights into intestinal stem cells. *Nature Reviews Gastroenterology & Hepatology.* 2019;16(1):19-34.
9. Barker N, Huch M, Kujala P, van de Wetering M, Snippert HJ, van Es JH, et al. Lgr5(+ve) stem cells drive self-renewal in the stomach and build long-lived gastric units in vitro. *Cell Stem Cell.* 2010;6(1):25-36.
10. Radtke F, and Clevers H. Self-Renewal and Cancer of the Gut: Two Sides of a Coin. 2005;307(5717):1904-9.
11. Sato T, Vries RG, Snippert HJ, van de Wetering M, Barker N, Stange DE, et al. Single Lgr5 stem cells build crypt–villus structures in vitro without a mesenchymal niche. *Nature.* 2009;459:262.
12. Schmitt M, Schewe M, Sacchetti A, Feijtel D, van de Geer WS, Teeuwssen M, et al. Paneth Cells Respond to Inflammation and Contribute to Tissue Regeneration by Acquiring Stem-like Features through SCF/c-Kit Signaling. *Cell Reports.* 2018;24(9):2312-28.e7.
13. Yu S, Tong K, Zhao Y, Balasubramanian I, Yap GS, Ferraris RP, et al. Paneth Cell Multipotency Induced by Notch Activation following Injury. *Cell Stem Cell.* 2018;23(1):46-59.e5.
14. Yan KS, Gevaert O, Zheng GXY, Anchang B, Probert CS, Larkin KA, et al. Intestinal Enteroendocrine Lineage Cells Possess Homeostatic and Injury-Inducible Stem Cell Activity. *Cell Stem Cell.* 2017;21(1):78-90.e6.
15. Sei Y, Feng J, Samsel L, White A, Zhao X, Yun S, et al. Mature enteroendocrine cells contribute to basal and pathological stem cell dynamics in the small intestine. 2018;315(4):G495-G510.
16. Westphalen CB, Asfaha S, Hayakawa Y, Takemoto Y, Lukin DJ, Nuber AH, et al. Long-lived intestinal tuft cells serve as colon cancer–initiating cells. *The Journal of Clinical Investigation.* 2014;124(3):1283-95.
17. Gerbe F, Brulin B, Makrini L, Legraverend C, and Jay P. DCAMKL-1 expression identifies Tuft cells rather than stem cells in the adult mouse intestinal epithelium. *Gastroenterology.* 2009;137(6):2179-80; author reply 80-1.
18. May R, Qu D, Weygant N, Chandrakesan P, Ali N, Lightfoot SA, et al. Brief report: Dclk1 deletion in tuft cells results in impaired epithelial repair after radiation injury. *Stem cells (Dayton, Ohio).* 2014;32(3):822-7.
19. Yi J, Bergstrom K, Fu J, Shan X, McDaniel JM, McGee S, et al. Dclk1 in tuft cells promotes inflammation-driven epithelial restitution and mitigates chronic colitis. *Cell death and differentiation.* 2018.

20. Tetteh Paul W, Basak O, Farin Henner F, Wiebrands K, Kretzschmar K, Begthel H, et al. Replacement of Lost Lgr5-Positive Stem Cells through Plasticity of Their Enterocyte-Lineage Daughters. *Cell Stem Cell.* 2016;18(2):203-13.
21. Yu J. Intestinal stem cell injury and protection during cancer therapy. *Translational cancer research.* 2013;2(5):384-96.
22. Johnson DI. Cdc42: An Essential Rho-Type GTPase Controlling Eukaryotic Cell Polarity. 1999;63(1):54-105.
23. Cardoso AP, Pinto ML, Pinto AT, Oliveira MI, Pinto MT, Goncalves R, et al. Macrophages stimulate gastric and colorectal cancer invasion through EGFR Y(1086), c-Src, Erk1/2 and Akt phosphorylation and smallGTPase activity. *Oncogene.* 2014;33(16):2123-33.
24. Al-Tassan NA, Whiffin N, Hosking FJ, Palles C, Farrington SM, Dobbins SE, et al. A new GWAS and meta-analysis with 1000Genomes imputation identifies novel risk variants for colorectal cancer. *Sci Rep.* 2015;5:10442.
25. Sakamori R, Yu S, Zhang X, Hoffman A, Sun J, Das S, et al. CDC42 inhibition suppresses progression of incipient intestinal tumors. *Cancer Res.* 2014;74(19):5480-92.
26. Wouters MM, Lambrechts D, Knapp M, Cleynen I, Whorwell P, Agreus L, et al. Genetic variants in CDC42 and NXPH1 as susceptibility factors for constipation and diarrhoea predominant irritable bowel syndrome. *Gut.* 2014;63(7):1103-11.
27. Wiegerinck CL, Janecke AR, Schneeberger K, Vogel GF, van Haaften-Visser DY, Escher JC, et al. Loss of syntaxin 3 causes variant microvillus inclusion disease. *Gastroenterology.* 2014;147(1):65-8.e10.
28. Sakamori R, Das S, Yu S, Feng S, Stypulkowski E, Guan Y, et al. Cdc42 and Rab8a are critical for intestinal stem cell division, survival, and differentiation in mice. *J Clin Invest.* 2012;122(3):1052-65.
29. Zhang X, and Gao N. RAB and RHO GTPases regulate intestinal crypt cell homeostasis and enterocyte function. *Small GTPases.* 2016;7(2):59-64.
30. Michaux G, Massey-Harroche D, Nicolle O, Rabant M, Brousse N, Goulet O, et al. The localisation of the apical Par/Cdc42 polarity module is specifically affected in microvillus inclusion disease. *Biol Cell.* 2016;108(1):19-28.
31. Yap K, Xiao Y, Friedman Brad A, Je HS, and Makeyev Eugene V. Polarizing the Neuron through Sustained Co-expression of Alternatively Spliced Isoforms. *Cell Reports.* 2016;15(6):1316-28.
32. Wirth A, Chen-Wacker C, Wu Y-W, Gorinski N, Filippov Mikhail A, Pandey G, et al. Dual lipidation of the brain-specific Cdc42 isoform regulates its functional properties. *Biochemical Journal.* 2013;456(3):311-22.
33. Nishimura A, and Linder ME. Identification of a novel prenyl and palmitoyl modification at the CaaX motif of Cdc42 that regulates RhoGDI binding. *Mol Cell Biol.* 2013;33(7):1417-29.
34. Mukai J, Tamura M, Fénelon K, Rosen Andrew M, Spellman Timothy J, Kang R, et al. Molecular Substrates of Altered Axonal Growth and Brain Connectivity in a Mouse Model of Schizophrenia. *Neuron.* 2015;86(3):680-95.
35. Kang R, Wan J, Arstikaitis P, Takahashi H, Huang K, Bailey AO, et al. Neural palmitoyl-proteomics reveals dynamic synaptic palmitoylation. *Nature.* 2008;456(7224):904-9.
36. Lee SJ, Kar AN, Kawaguchi R, Patel P, Sahoo PK, Aguilar B, et al. Selective axonal translation of prenylated Cdc42 mRNA isoform supports axon growth. *bioRxiv.* 2018.
37. Sigismund S, Argenzio E, Tosoni D, Cavallaro E, Polo S, and Di Fiore PP. Clathrin-Mediated Internalization Is Essential for Sustained EGFR Signaling but Dispensable for Degradation. *Developmental Cell.* 2008;15(2):209-19.
38. Henriksen L, Grandal MV, Knudsen SLJ, van Deurs B, and Grøvdal LM. Internalization Mechanisms of the Epidermal Growth Factor Receptor after Activation with Different Ligands. *PLOS ONE.* 2013;8(3):e58148.

39. Goh LK, Huang F, Kim W, Gygi S, and Sorkin A. Multiple mechanisms collectively regulate clathrin-mediated endocytosis of the epidermal growth factor receptor. *The Journal of Cell Biology.* 2010;189(5):871.
40. Huang F, Khvorova A, Marshall W, and Sorkin A. Analysis of Clathrin-mediated Endocytosis of Epidermal Growth Factor Receptor by RNA Interference. 2004;279(16):16657-61.
41. Vehlow A, Soong D, Vizcay-Barrena G, Bodo C, Law A-L, Perera U, et al. Endophilin, Lamellipodin, and Mena cooperate to regulate F-actin-dependent EGF-receptor endocytosis. *The EMBO journal.* 2013;32(20):2722-34.
42. Zhang X, Ren J, Wang J, Li S, Zou Q, and Gao N. Receptor-mediated endocytosis generates nanomechanical force reflective of ligand identity and cellular property. 2018;233(8):5908-19.
43. Macia E, Ehrlich M, Massol R, Boucrot E, Brunner C, and Kirchhausen T. Dynasore, a Cell-Permeable Inhibitor of Dynamin. *Developmental Cell.* 2006;10(6):839-50.
44. Yun M-S, Kim S-E, Jeon SH, Lee J-S, and Choi K-Y. Both ERK and Wnt/β-catenin pathways are involved in Wnt3a-induced proliferation. *Journal of Cell Science.* 2005;118(2):313.
45. Davis CR, Richman TJ, Deliduka SB, Blaisdell JO, Collins CC, and Johnson DI. Analysis of the mechanisms of action of the Saccharomyces cerevisiae dominant lethal cdc42G12V and dominant negative cdc42D118A mutations. *J Biol Chem.* 1998;273(2):849-58.
46. Johnson DI. Cdc42: An essential Rho-type GTPase controlling eukaryotic cell polarity. *Microbiology and molecular biology reviews : MMBR.* 1999;63(1):54-105.
47. Johnson JL, Erickson JW, and Cerione RA. C-terminal di-arginine motif of Cdc42 protein is essential for binding to phosphatidylinositol 4,5-bisphosphate-containing membranes and inducing cellular transformation. *The Journal of biological chemistry.* 2012;287(8):5764-74.
48. Yang YP, Ma H, Starchenko A, Huh WJ, Li W, Hickman FE, et al. A Chimeric Egfr Protein Reporter Mouse Reveals Egfr Localization and Trafficking In Vivo. *Cell Rep.* 2017;19(6):1257-67.
49. Irwin ME, Mueller KL, Bohin N, Ge Y, and Boerner JL. Lipid raft localization of EGFR alters the response of cancer cells to the EGFR tyrosine kinase inhibitor gefitinib. 2011;226(9):2316-28.
50. Hofman EG, Ruonala MO, Bader AN, van den Heuvel D, Voortman J, Roovers RC, et al. EGF induces coalescence of different lipid rafts. *Journal of Cell Science.* 2008;121(15):2519.
51. Patra SK. Dissecting lipid raft facilitated cell signaling pathways in cancer. *Biochimica et Biophysica Acta (BBA) - Reviews on Cancer.* 2008;1785(2):182-206.
52. Pike LJ, Han X, and Gross RW. Epidermal Growth Factor Receptors Are Localized to Lipid Rafts That Contain a Balance of Inner and Outer Leaflet Lipids: A SHOTGUN LIPIDOMICS STUDY. 2005;280(29):26796-804.
53. Puri C, Tosoni D, Comai R, Rabellino A, Segat D, Caneva F, et al. Relationships between EGFR Signaling–competent and Endocytosis-competent Membrane Microdomains. *Molecular Biology of the Cell.* 2005;16(6):2704-18.
54. Bruckner K, Pablo Labrador J, Scheiffele P, Herb A, Seeburg PH, and Klein R. EphrinB ligands recruit GRIP family PDZ adaptor proteins into raft membrane microdomains. *Neuron.* 1999;22(3):511-24.
55. Salzer U, and Prohaska R. Stomatin, flotillin-1, and flotillin-2 are major integral proteins of erythrocyte lipid rafts. *Blood.* 2001;97(4):1141-3.
56. Rothberg KG, Heuser JE, Donzell WC, Ying YS, Glenney JR, and Anderson RG. Caveolin, a protein component of caveolae membrane coats. *Cell.* 1992;68(4):673-82.
57. Pereira DB, and Chao MV. The tyrosine kinase Fyn determines the localization of TrkB receptors in lipid rafts. *The Journal of neuroscience : the official journal of the Society for Neuroscience.* 2007;27(18):4859-69.
58. Gao X, Lowry PR, Zhou X, Depry C, Wei Z, Wong GW, et al. PI3K/Akt signaling requires spatial compartmentalization in plasma membrane microdomains. 2011;108(35):14509-14.

59. Yamamoto H, Komekado H, and Kikuchi A. Caveolin is necessary for Wnt-3a-dependent internalization of LRP6 and accumulation of beta-catenin. *Dev Cell.* 2006;11(2):213-23.
60. Bilic J, Huang YL, Davidson G, Zimmermann T, Cruciat CM, Bienz M, et al. Wnt induces LRP6 signalosomes and promotes dishevelled-dependent LRP6 phosphorylation. *Science.* 2007;316(5831):1619-22.
61. McNulty DE, Li Z, White CD, Sacks DB, and Annan RS. MAPK scaffold IQGAP1 binds the EGF receptor and modulates its activation. *J Biol Chem.* 2011;286(17):15010-21.
62. Bikkavilli RK, Feigin ME, and Malbon CC. p38 mitogen-activated protein kinase regulates canonical Wnt-beta-catenin signaling by inactivation of GSK3beta. *J Cell Sci.* 2008;121(Pt 21):3598-607.
63. Holowka D, and Baird B. Mechanisms of epidermal growth factor receptor signaling as characterized by patterned ligand activation and mutational analysis. *Biochim Biophys Acta Biomembr.* 2017;1859(9 Pt A):1430-5.
64. Sigismund S, Argenzio E, Tosoni D, Cavallaro E, Polo S, and Di Fiore PP. Clathrin-mediated internalization is essential for sustained EGFR signaling but dispensable for degradation. *Dev Cell.* 2008;15(2):209-19.
65. Siu MK, Chan HY, Kong DS, Wong ES, Wong OG, Ngan HY, et al. p21-activated kinase 4 regulates ovarian cancer cell proliferation, migration, and invasion and contributes to poor prognosis in patients. *Proc Natl Acad Sci U S A.* 2010;107(43):18622-7.
66. Yin X, Farin HF, van Es JH, Clevers H, Langer R, and Karp JM. Niche-independent high-purity cultures of Lgr5+ intestinal stem cells and their progeny. *Nat Methods.* 2014;11(1):106-12.
67. Kishida K, Pearce SC, Yu S, Gao N, and Ferraris RP. Nutrient sensing by absorptive and secretory progenies of small intestinal stem cells. *American journal of physiology Gastrointestinal and liver physiology.* 2017;312(6):G592-G605.
68. Weaver LT, Austin S, and Cole TJ. Small intestinal length: a factor essential for gut adaptation. *Gut.* 1991;32(11):1321-3.
69. Riehl TE, Ee X, and Stenson WF. Hyaluronic acid regulates normal intestinal and colonic growth in mice. *American Journal of Physiology-Gastrointestinal and Liver Physiology.* 2012;303(3):G377-G88.
70. Heuberger J, Kosel F, Qi J, Grossmann KS, Rajewsky K, and Birchmeier W. Shp2/MAPK signaling controls goblet/paneth cell fate decisions in the intestine. *Proceedings of the National Academy of Sciences.* 2014;111(9):3472.
71. Geske MJ, Zhang X, Patel KK, Ornitz DM, and Stappenbeck TS. Fgf9 signaling regulates small intestinal elongation and mesenchymal development. *Development.* 2008;135(17):2959.
72. Potten CS. Extreme sensitivity of some intestinal crypt cells to X and γ irradiation. *Nature.* 1977;269:518.
73. Kim C-K, Yang VW, and Bialkowska AB. The Role of Intestinal Stem Cells in Epithelial Regeneration Following Radiation-Induced Gut Injury. *Current stem cell reports.* 2017;3(4):320-32.
74. Metcalfe C, Kljavin Noelyn M, Ybarra R, and de Sauvage Frederic J. Lgr5⁺ Stem Cells Are Indispensable for Radiation-Induced Intestinal Regeneration. *Cell Stem Cell.* 2014;14(2):149-59.
75. Gong W, Guo M, Han Z, Wang Y, Yang P, Xu C, et al. Mesenchymal stem cells stimulate intestinal stem cells to repair radiation-induced intestinal injury. *Cell Death &Amp; Disease.* 2016;7:e2387.
76. Gomez Del Pulgar T, Valdes-Mora F, Bandres E, Perez-Palacios R, Espina C, Cejas P, et al. Cdc42 is highly expressed in colorectal adenocarcinoma and downregulates ID4 through an epigenetic mechanism. *Int J Oncol.* 2008;33(1):185-93.
77. Abe K, Rossman KL, Liu B, Ritola KD, Chiang D, Campbell SL, et al. Vav2 is an activator of Cdc42, Rac1, and RhoA. *J Biol Chem.* 2000;275(14):10141-9.
78. Tapon N, and Hall A. Rho, Rac and Cdc42 GTPases regulate the organization of the actin cytoskeleton. *Curr Opin Cell Biol.* 1997;9(1):86-92.

79. Threadgill R, Bobb K, and Ghosh A. Regulation of dendritic growth and remodeling by Rho, Rac, and Cdc42. *Neuron.* 1997;19(3):625-34.
80. Wojciak-Stothard B, and Ridley AJ. Shear stress-induced endothelial cell polarization is mediated by Rho and Rac but not Cdc42 or PI 3-kinases. *J Cell Biol.* 2003;161(2):429-39.
81. Moreau V, and Way M. Cdc42 is required for membrane dependent actin polymerization in vitro. *FEBS Lett.* 1998;427(3):353-6.
82. Warner SJ, and Longmore GD. Cdc42 antagonizes Rho1 activity at adherens junctions to limit epithelial cell apical tension. *J Cell Biol.* 2009;187(1):119-33.
83. Li Z, Aizenman CD, and Cline HT. Regulation of rho GTPases by crosstalk and neuronal activity in vivo. *Neuron.* 2002;33(5):741-50.
84. Dise RS, Frey MR, Whitehead RH, and Polk DB. Epidermal growth factor stimulates Rac activation through Src and phosphatidylinositol 3-kinase to promote colonic epithelial cell migration. *Am J Physiol Gastrointest Liver Physiol.* 2008;294(1):G276-85.
85. Slice LW, Chiu T, and Rozengurt E. Angiotensin II and epidermal growth factor induce cyclooxygenase-2 expression in intestinal epithelial cells through small GTPases using distinct signaling pathways. *J Biol Chem.* 2005;280(2):1582-93.
86. Jiang H, and Edgar BA. EGFR signaling regulates the proliferation of Drosophila adult midgut progenitors. *Development.* 2009;136(3):483-93.
87. Jiang H, Grenley MO, Bravo MJ, Blumhagen RZ, and Edgar BA. EGFR/Ras/MAPK signaling mediates adult midgut epithelial homeostasis and regeneration in Drosophila. *Cell Stem Cell.* 2011;8(1):84-95.
88. Xu N, Wang SQ, Tan D, Gao Y, Lin G, and Xi R. EGFR, Wingless and JAK/STAT signaling cooperatively maintain Drosophila intestinal stem cells. *Dev Biol.* 2011;354(1):31-43.
89. Pyo JH, Jeon HJ, Park JS, Lee JS, Chung HY, and Yoo MA. Drosophila PEBP1 inhibits intestinal stem cell aging via suppression of ERK pathway. *Oncotarget.* 2018;9(26):17980-93.
90. Buchon N, Broderick NA, Kuraishi T, and Lemaitre B. Drosophila EGFR pathway coordinates stem cell proliferation and gut remodeling following infection. *BMC Biol.* 2010;8:152.
91. Jin Y, Ha N, Fores M, Xiang J, Glasser C, Maldera J, et al. EGFR/Ras Signaling Controls Drosophila Intestinal Stem Cell Proliferation via Capicua-Regulated Genes. *PLoS Genet.* 2015;11(12):e1005634.
92. Jiang H, Tian A, and Jiang J. Intestinal stem cell response to injury: lessons from Drosophila. *Cell Mol Life Sci.* 2016;73(17):3337-49.
93. Mytych J, Satora L, and Koziol K. Confirmation of the immunoreactivity of monoclonal anti-human C-terminal EGFR antibodies in bronze Corydoras Corydoras aeneus (Callichthyidae Teleostei) by Western Blot method. *Acta Histochem.* 2018;120(2):151-3.
94. Satora L, Mytych J, and Bilska-Kos A. The presence and expression of the HIF-1alpha in the respiratory intestine of the bronze Corydoras Corydoras aeneus (Callichthyidae Teleostei). *Fish Physiol Biochem.* 2018;44(5):1291-7.
95. Liang J, Balachandra S, Ngo S, and O'Brien LE. Feedback regulation of steady-state epithelial turnover and organ size. *Nature.* 2017;548(7669):588-91.
96. Cordero JB, Ridgway RA, Valeri N, Nixon C, Frame MC, Muller WJ, et al. c-Src drives intestinal regeneration and transformation. *EMBO J.* 2014;33(13):1474-91.
97. Suzuki A, Sekiya S, Gunshima E, Fujii S, and Taniguchi H. EGF signaling activates proliferation and blocks apoptosis of mouse and human intestinal stem/progenitor cells in long-term monolayer cell culture. *Lab Invest.* 2010;90(10):1425-36.
98. Takeda H, and Kiyokawa E. Activation of Erk in ileal epithelial cells engaged in ischemic-injury repair. *Scientific reports.* 2017;7(1):16469.
99. Miguel JC, Maxwell AA, Hsieh JJ, Harnisch LC, Al Alam D, Polk DB, et al. Epidermal growth factor suppresses intestinal epithelial cell shedding through a MAPK-dependent pathway. *J Cell Sci.* 2017;130(1):90-6.

100. Ungewiss H, Rotzer V, Meir M, Fey C, Diefenbacher M, Schlegel N, et al. Dsg2 via Src-mediated transactivation shapes EGFR signaling towards cell adhesion. *Cell Mol Life Sci.* 2018;75(22):4251-68.
101. Gregorieff A, Liu Y, Inanlou MR, Khomchuk Y, and Wrana JL. Yap-dependent reprogramming of Lgr5(+) stem cells drives intestinal regeneration and cancer. *Nature.* 2015;526(7575):715-8.
102. Ren F, Wang B, Yue T, Yun EY, Ip YT, and Jiang J. Hippo signaling regulates Drosophila intestine stem cell proliferation through multiple pathways. *Proc Natl Acad Sci U S A.* 2010;107(49):21064-9.
103. Zhang Y, Pizzute T, and Pei M. A review of crosstalk between MAPK and Wnt signals and its impact on cartilage regeneration. *Cell Tissue Res.* 2014;358(3):633-49.
104. Bikkavilli RK, Feigin ME, and Malbon CC. G alpha o mediates WNT-JNK signaling through dishevelled 1 and 3, RhoA family members, and MEKK 1 and 4 in mammalian cells. *J Cell Sci.* 2008;121(Pt 2):234-45.
105. Yun MS, Kim SE, Jeon SH, Lee JS, and Choi KY. Both ERK and Wnt/beta-catenin pathways are involved in Wnt3a-induced proliferation. *J Cell Sci.* 2005;118(Pt 2):313-22.
106. Batlle E, Henderson JT, Beghtel H, van den Born MM, Sancho E, Huls G, et al. Beta-catenin and TCF mediate cell positioning in the intestinal epithelium by controlling the expression of EphB/ephrinB. *Cell.* 2002;111(2):251-63.
107. Kim IH, Wang H, Soderling SH, and Yasuda R. Loss of Cdc42 leads to defects in synaptic plasticity and remote memory recall. *eLife.* 2014;3.
108. Moutin E, Nikonenko I, Stefanelli T, Wirth A, Ponimaskin E, De Roo M, et al. Palmitoylation of cdc42 Promotes Spine Stabilization and Rescues Spine Density Deficit in a Mouse Model of 22q11.2 Deletion Syndrome. *Cerebral cortex (New York, NY : 1991).* 2017;27(7):3618-29.
109. Mukai J, Dhilla A, Drew LJ, Stark KL, Cao L, MacDermott AB, et al. Palmitoylation-dependent neurodevelopmental deficits in a mouse model of 22q11 microdeletion. *Nat Neurosci.* 2008;11(11):1302-10.
110. Mukai J, Tamura M, Fenelon K, Rosen AM, Spellman TJ, Kang R, et al. Molecular substrates of altered axonal growth and brain connectivity in a mouse model of schizophrenia. *Neuron.* 2015;86(3):680-95.
111. Tong K, Pellon-Cardenas O, Sirihorachai VR, Warder BN, Kothari OA, Perekatt AO, et al. Degree of Tissue Differentiation Dictates Susceptibility to BRAF-Driven Colorectal Cancer. *Cell Rep.* 2017;21(13):3833-45.
112. Heuberger J, Kosel F, Qi J, Grossmann KS, Rajewsky K, and Birchmeier W. Shp2/MAPK signaling controls goblet/paneth cell fate decisions in the intestine. *Proc Natl Acad Sci U S A.* 2014;111(9):3472-7.
113. Wu X, Quondamatteo F, Lefever T, Czuchra A, Meyer H, Chrostek A, et al. Cdc42 controls progenitor cell differentiation and β-catenin turnover in skin. *Genes & Development.* 2006;20(5):571-85.
114. Madison BB, Dunbar L, Qiao XT, Braunstein K, Braunstein E, and Gumucio DL. Cis elements of the villin gene control expression in restricted domains of the vertical (crypt) and horizontal (duodenum, cecum) axes of the intestine. *J Biol Chem.* 2002;277(36):33275-83.
115. El Marjou F, Janssen K-P, Hung-Junn Chang B, Li M, Hindie V, Chan L, et al. Tissue-specific and inducible Cre-mediated recombination in the gut epithelium. *genesis.* 2004;39(3):186-93.
116. Barker N, van Es JH, Kuipers J, Kujala P, van den Born M, Cozijnsen M, et al. Identification of stem cells in small intestine and colon by marker gene Lgr5. *Nature.* 2007;449(7165):1003-7.
117. Madisen L, Zwingman TA, Sunkin SM, Oh SW, Zariwala HA, Gu H, et al. A robust and high-throughput Cre reporting and characterization system for the whole mouse brain. *Nat Neurosci.* 2010;13(1):133-40.
118. Bohin N, Carlson EA, and Samuelson LC. Genome Toxicity and Impaired Stem Cell Function after Conditional Activation of CreER(T2) in the Intestine. *Stem Cell Reports.* 2018;11(6):1337-46.

119. Gregorieff A, and Clevers H. In situ hybridization to identify gut stem cells. *Curr Protoc Stem Cell Biol.* 2010;Chapter 2:Unit 2F 1.
120. Bean DM, Heimbach J, Ficorella L, Micklem G, Oliver SG, and Favrin G. esyN: network building, sharing and publishing. *PLoS One.* 2014;9(9):e106035.
121. Subramanian A, Tamayo P, Mootha VK, Mukherjee S, Ebert BL, Gillette MA, et al. Gene set enrichment analysis: A knowledge-based approach for interpreting genome-wide expression profiles. *Proceedings of the National Academy of Sciences.* 2005;102(43):15545-50.
122. Mootha VK, Lindgren CM, Eriksson K-F, Subramanian A, Sihag S, Lehar J, et al. PGC-1α-responsive genes involved in oxidative phosphorylation are coordinately downregulated in human diabetes. *Nature Genetics.* 2003;34(3):267-73.
123. Jia Z, Zhang X, Guan N, Bo X, Barnes MR, and Luo Z. Gene Ranking of RNA-Seq Data via Discriminant Non-Negative Matrix Factorization. *PLOS ONE.* 2015;10(9):e0137782.
124. Munoz J, Stange DE, Schepers AG, van de Wetering M, Koo BK, Itzkovitz S, et al. The Lgr5 intestinal stem cell signature: robust expression of proposed quiescent '+4' cell markers. *Embo J.* 2012;31(14):3079-91.

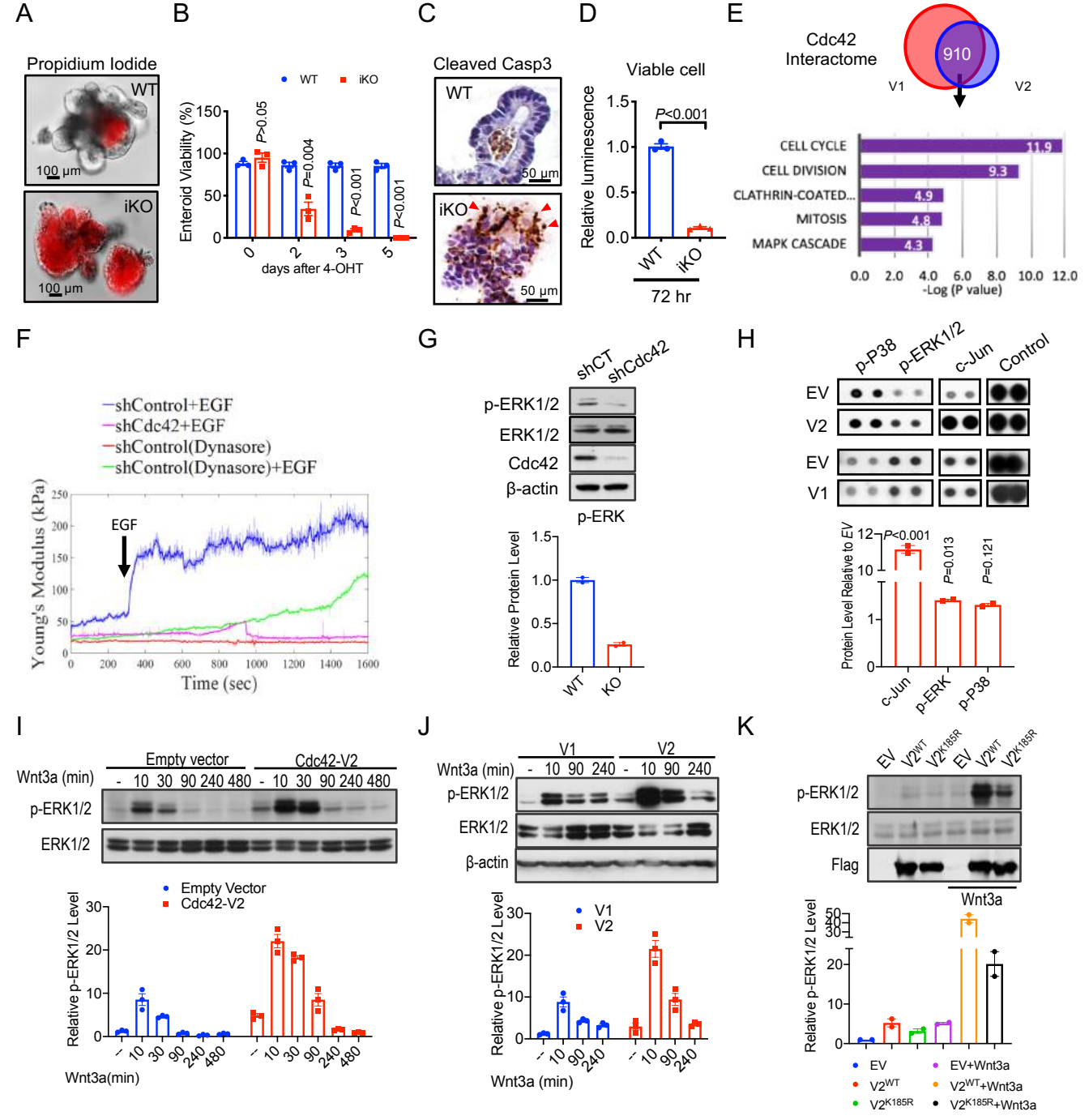
A
Propidium Iodide
WT
100 μm
iKO
100 μm
B
WT
iKO
Enteroid Viability (%)
150
100
50
0
P>0.05
P=0.004
P<0.001
P<0.001
0
2
3
5
days after 4-OHT
C
Cleaved Casp3
WT
50 μm
iKO
50 μm
D
Viable cell
Relative luminescence
1.5
1.0
0.5
0.0
P<0.001
WT
iKO
72 hr
E
Cdc42
Interactome
910
V1
V2
CELL CYCLE
11.9
CELL DIVISION
9.3
CLATHRIN-COATED...
4.9
MITOSIS
4.8
MAPK CASCADE
4.3
0.0 2.0 4.0 6.0 8.0 10.0 12.0
-Log (P value)
F
shControl+EGF
shCdc42+EGF
shControl(Dynasore)
shControl(Dynasore)+EGF
Young's Modulus (kPa)
EGF
Time (sec)
G
shCT
shCdc42
p-ERK1/2
ERK1/2
Cdc42
β-actin
p-ERK
Relative Protein Level
WT
KO
H
p-P38
p-ERK1/2
c-Jun
Control
EV
V2
EV
V1
Protein Level Relative to EV
P<0.001
P=0.013
P=0.121
c-Jun
p-ERK
p-P38
I
Empty vector
Cdc42-V2
Wnt3a (min)
- 10 30 90 240 480 - 10 30 90 240 480
p-ERK1/2
ERK1/2
Empty Vector
Cdc42-V2
Relative p-ERK1/2 Level
Wnt3a(min)
J
V1
V2
Wnt3a (min)
- 10 90 240 - 10 90 240
p-ERK1/2
ERK1/2
β-actin
V1
V2
Relative p-ERK1/2 Level
Wnt3a (min)
K
EV
V2WT
V2K185R
EV
V2WT
V2K185R
p-ERK1/2
ERK1/2
Flag
Wnt3a
Relative p-ERK1/2 Level
EV
V2WT
V2K185R
EV+Wnt3a
V2WT+Wnt3a
V2K185R+Wnt3a

Figure 1. Enteroid survival requires Cdc42 for EGF-MAPK signaling.

(A) 72 hrs after 4-OHT treatment of WT and Cdc42-iKO enteroids, propidium iodide staining (red) showed massive cell death.

(B) After 4-OHT treatment of enteroids, viable enteroids were counted at day 2, 3 and 5 following treatment. Data represents 3 independent experiments each containing 2 replicates per genotype.

(C) WT and Cdc42-iKO enteroid sections were stained for cleaved Caspase 3 to detect apoptotic cells. Images shown represented 72 hrs after treatment.

(D) 3D-Glo luminescent assays were used to quantify cell viability in WT and Cdc42-iKO enteroids 72 hrs after 4-OHT treatment. Data represents two independent experiments each containing 2 replicates per genotype.

(E) HEK293 cells were transfected with Flag-tagged Cdc42 V1 or V2. Mass spectrometry analysis of Flag-Cdc42 immunoprecipitates identified variant-specific interactome. Venn diagram reveals 910 shared interactors. Functional annotation showed the top 5 most enriched clusters ranked by p-value by NIH DAVID.

(F) Serum-starved Caco2 control and Cdc42 knockdown cells were analyzed by atomic force microscope. EGF was added to cells 300 sec after recording of each sample. Young's modulus (kPa) indicated EGF-induced nanomechanical changes on control Caco2 cell surface, diminished responses in control cells pre-incubated with dynasore or in Cdc42 knockdown cells. Graphs represented 4 independent experiments.

(G) Western blots for p-ERK1/2 were performed for control and stable Cdc42-knockdown Caco2 cells cultured in regular medium with no treatment. Data were quantified from 2 independent experiments.

(H) Phospho-kinase array was used to search for functional pathways downstream of Cdc42. Among 43 kinase targets, overexpressing Cdc42 in HEK293 cells increased levels of phosphorylated ERK1/2, p38 and c-Jun, especially in V2-expressing cells compared to empty vector controls. Graph represented mean values from 2 replicates.

(I) Western blots were used to determine change of p-ERK1/2 in serum-starved control and Cdc42-V2 expressing cells, following the addition of Wnt3a (100ng/ml), on time course experiments.

(J) Western blots for p-ERK1/2 were used to compare V1 vs. V2's MAPK-activating capabilities.

(K) Mutant Cdc42-V2$_{K185R}$ showed a reduced MAPK-activating capability compared to WT Cdc42-V2. Data were quantified from 2 independent experiments in I, J, and K.

Please also see Suppl. Figure 1.

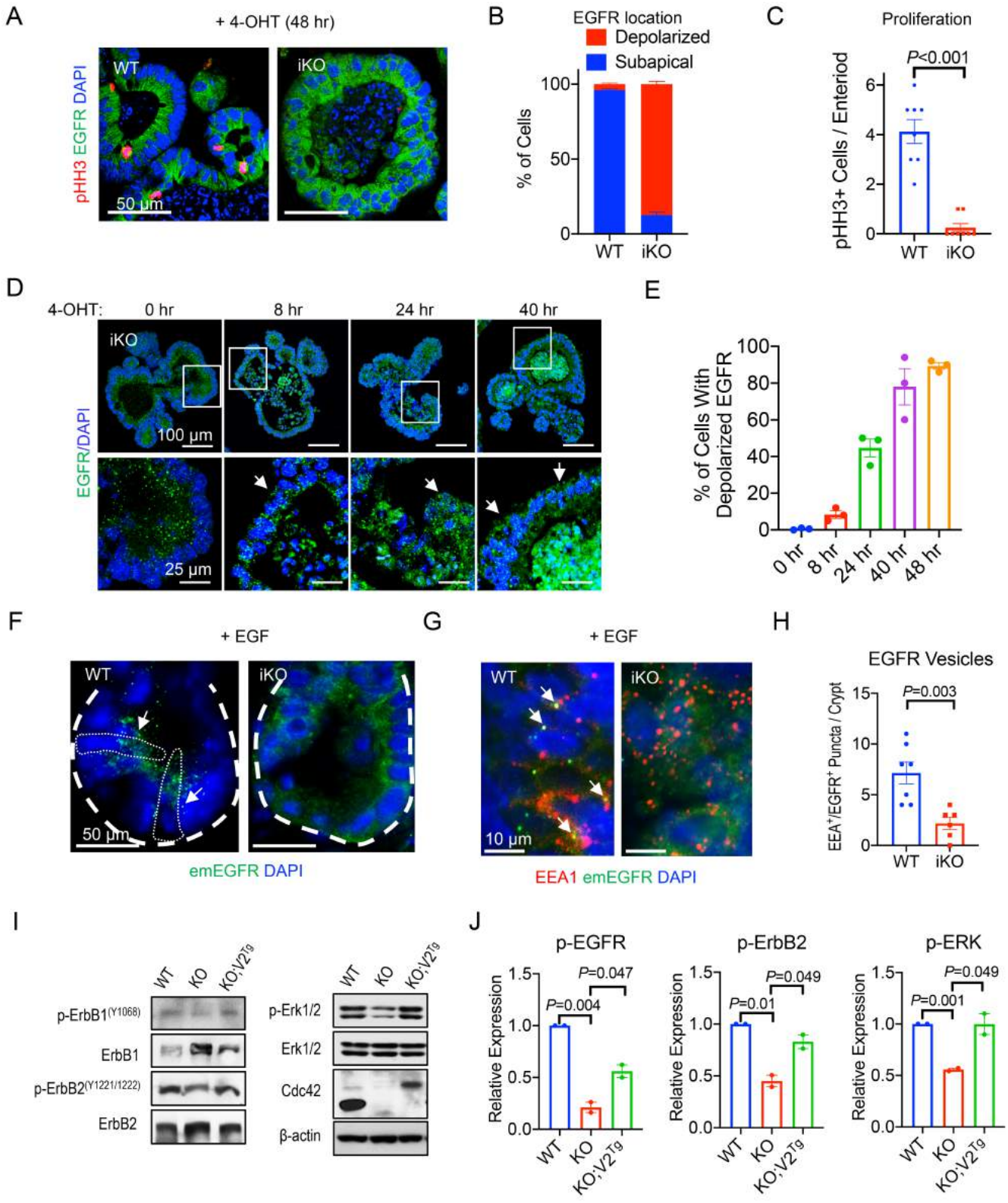
A
+ 4-OHT (48 hr)
WT
iKO
pHH3 EGFR DAPI
50 μm
B
EGFR location
Depolarized
Subapical
% of Cells
100
50
0
WT
iKO
C
Proliferation
P<0.001
pHH3+ Cells / Enteriod
6
4
2
0
WT
iKO
D
4-OHT:
0 hr
8 hr
24 hr
40 hr
iKO
EGFR/DAPI
100 μm
25 μm
E
% of Cells With Depolarized EGFR
100
80
60
40
20
0
0 hr
8 hr
24 hr
40 hr
48 hr
F
+ EGF
WT
iKO
50 μm
emEGFR DAPI
G
+ EGF
WT
iKO
10 μm
EEA1 emEGFR DAPI
H
EGFR Vesicles
P=0.003
EEA+/EGFR+ Puncta / Crypt
15
10
5
0
WT
iKO
I
WT
KO
KO;V2Tg
p-ErbB1(Y1068)
ErbB1
p-ErbB2(Y1221/1222)
ErbB2
p-Erk1/2
Erk1/2
Cdc42
β-actin
J
p-EGFR
p-ErbB2
p-ERK
Relative Expression
1.5
1.0
0.5
0.0
P=0.004
P=0.047
P=0.01
P=0.049
P=0.001
P=0.049
WT
KO
KO;V2Tg

Figure 2. Cdc42 is indispensable for EGFR endocytosis.

(A) WT and Cdc42-iKO enteroids were treated with 4-OHT for 48 hrs. Enteroid sections were stained for endogenous EGFR (green) and mitosis marker (pHH3, red).

(B) Quantification of intracellular localization of EGFR in WT and Cdc42-iKO enteroid cells, based on immunofluorescent staining of EGFR in 4-OHT treated enteroids (48 hrs).

(C) $pHH3^{+}$ cell number was quantified per enteroid. Data in B-C were quantified from 2 independent experiments.

(D) Enteroid sections were stained for EGFR after 4-OHT treatment at 8, 24, and 40 hr. White arrows pointed to delocalized EGFR compared to EGFR localization in untreated enteroids.

(E) Quantification of percentage of cells showing changed EGFR localization at indicated time points after 4-OHT addition.

(F) Cdc42 mice were crossed to emerald-EGFR mice to visualize EGFR. 30-min after EGF injection, Emerald-EGFR vesicles (green, white arrows) were seen in Cdc42-WT mouse crypt cells; but were barely detected in iKO crypt cells. White dotted circles indicated crypt base stem cells.

(G-H) Double fluorescent analysis for EEA1 (red) and emerald-EGFR (green, white arrows) detected endocytic EGFR in WT crypt cells but not Cdc42 iKO cells 30 min after EGF injection. $EEA1^{+}/EGFR^{+}$ puncta per crypt were quantified from 4 mice in 2 independent experiments.

(I-J) Western blots for endogenous pErbB1 (Y1068), pErbB2 (Y1221/1222), and p-Erk1/2 were performed for WT, Cdc42 KO, and Cdc42-$V2_{Tg}$ mouse intestines. Data represented 2 independent experiments.

Please also see Suppl. Figure 2.

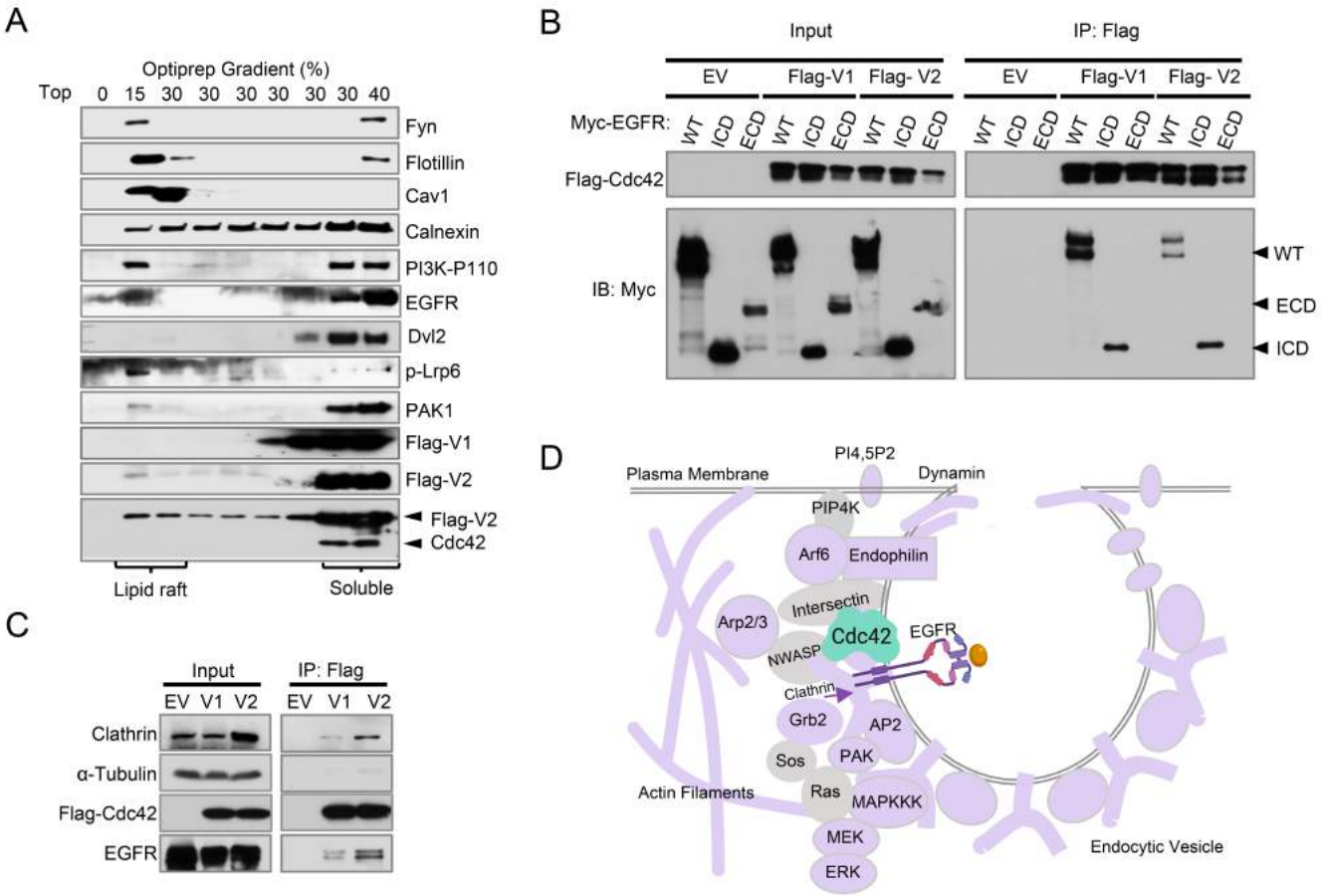
A
Optiprep Gradient (%)
Top 0 15 30 30 30 30 30 40
Fyn
Flotillin
Cav1
Calnexin
PI3K-P110
EGFR
Dvl2
p-Lrp6
PAK1
Flag-V1
Flag-V2
Flag-V2
Cdc42
Lipid raft
Soluble
B
Input
IP: Flag
EV
Flag-V1
Flag- V2
Myc-EGFR:
WT ICD ECD WT ICD ECD WT ICD ECD WT ICD ECD WT ICD ECD
Flag-Cdc42
IB: Myc
WT
ECD
ICD
C
Input
IP: Flag
EV V1 V2 EV V1 V2
Clathrin
α-Tubulin
Flag-Cdc42
EGFR
D
PI4,5P2
Plasma Membrane
Dynamin
PIP4K
Arf6
Endophilin
Intersectin
Arp2/3
Cdc42
EGFR
NWASP
Clathrin
Grb2
AP2
Sos
PAK
Actin Filaments
Ras
MAPKKK
MEK
ERK
Endocytic Vesicle

Figure 3. Cdc42 engages EGFR and endocytosis machinery.

(A) Optiprep gradient cellular fractionation of HEK293 cells showed co-sedimentation of Cdc42-V2 with EGFR, p-LRP6, and PI3K-P110 in lipid raft fractions marked Fyn, Cav1, and Flotillin. Calnexin is an ER marker. Data represented 3 independent experiments.

(B) Co-immunoprecipitation analysis showed that Flag-tagged Cdc42 associated with full length EGFR and EGFR intracellular domain (ICD), but not the extracellular domain (ECD) in HEK293 cells.

(C) Co-immunoprecipitation analysis showed that, compared to V1, V2 exhibited a stronger interaction with endogenous EGFR and clathrin in HEK293 cells.

(D) A diagram illustrating the structural and functional protein components found in Cdc42 proteomics that were known to regulate clathrin-mediated trafficking, EGFR endocytosis, and MAPK cascade.

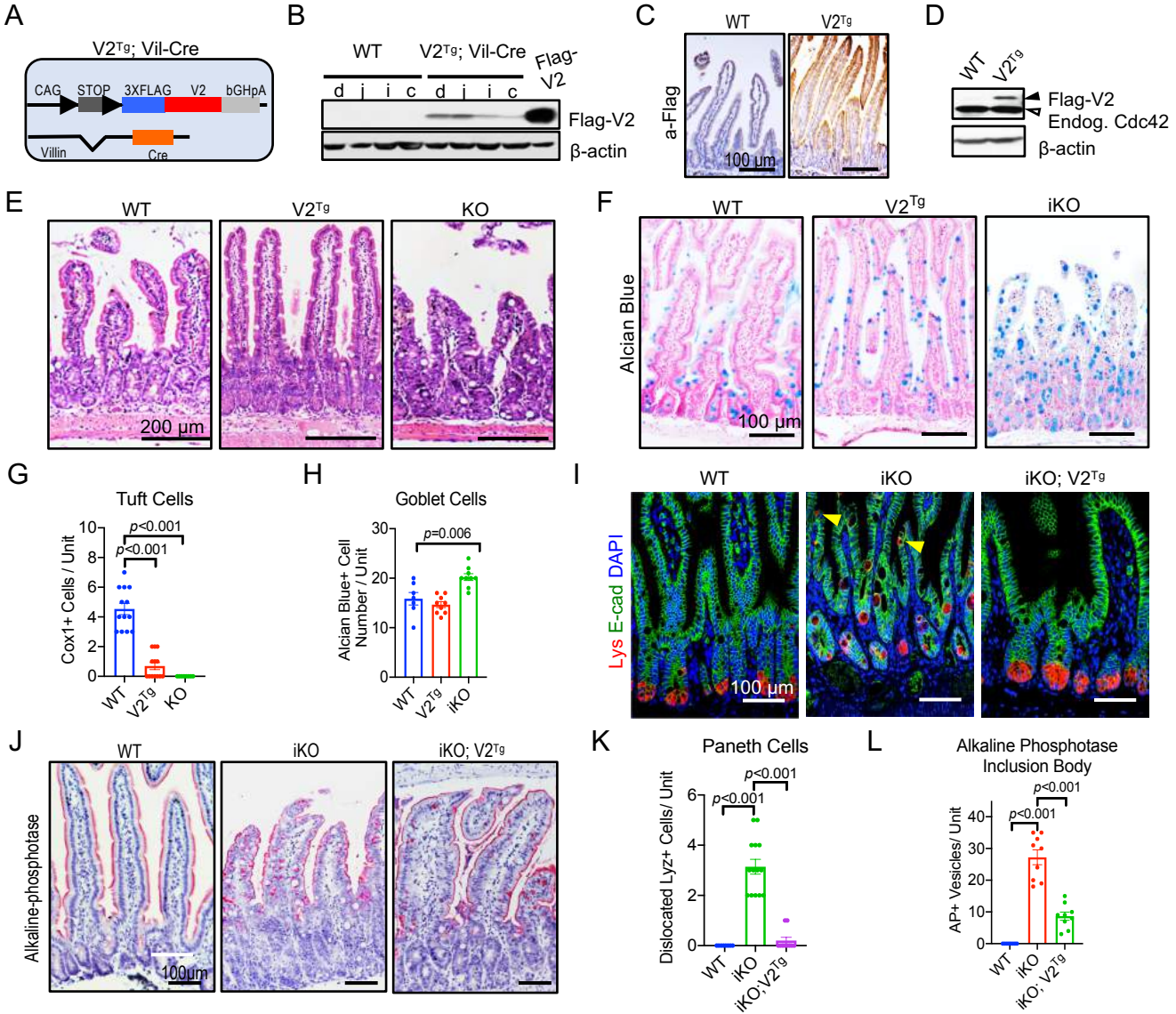
A
V2Tg; Vil-Cre
CAG
STOP
3XFLAG
V2
bGHpA
Villin
Cre
B
WT
V2Tg; Vil-Cre
Flag-V2
d j i c d j i c
Flag-V2
β-actin
C
WT
V2Tg
a-Flag
100 μm
D
WT
V2Tg
Flag-V2
Endog. Cdc42
β-actin
E
WT
V2Tg
KO
200 μm
F
WT
V2Tg
iKO
Alcian Blue
100 μm
G
Tuft Cells
Cox1+ Cells / Unit
p<0.001
p<0.001
WT
V2Tg
KO
H
Goblet Cells
Alcian Blue+ Cell Number / Unit
p=0.006
WT
V2Tg
iKO
I
WT
iKO
iKO; V2Tg
Lys E-cad DAPI
100 μm
J
WT
iKO
iKO; V2Tg
Alkaline-phosphotase
100μm
K
Paneth Cells
Dislocated Lyz+ Cells/ Unit
p<0.001
p<0.001
WT
iKO
iKO;V2Tg
L
Alkaline Phosphotase Inclusion Body
AP+ Vesicles/ Unit
p<0.001
p<0.001
WT
iKO
iKO; V2Tg

Figure 4. Overexpressing Cdc42 V2 in mouse intestinal epithelium impacts differentiation.

(A) A schematic diagram showing the strategy of developing a Cdc42 $V2_{Tg}$ mouse allele, which conditionally expressed a Flag-tagged Cdc42-V2 in a Cre-dependent manner. A loxP-stop-loxP-3xFlag-V2-bGHpolyA cassette was inserted downstream of a CAG promoter.

(B) Western blots for Flag detected Flag-V2 expression in duodenum, jejunum, ileum, and colon of $V2_{Tg}$ driven by Vil-Cre. HEK293 cells expressing Flag-V2 was used as positive control.

(C) Immunohistochemistry for Flag detected Flag-V2 expression in $V2_{Tg}$ mouse IECs. Images are representative of 3 independent mice per genotype.

(D) Western blots for Cdc42 showed that the transgenic expression of V2 (upper band) in a $V2_{Tg}$ line was approximately 40% of endogenous Cdc42 (empty arrowhead).

(E) H&E staining of mouse intestines. $V2_{Tg}$ small intestines showed longer villi and more crypts; KO showed blunted villi.

(F) Alcian Blue staining of mouse intestinal sections of indicated genotypes.

(G) Quantification of Cox1+ cell number per crypt-villus unit.

(H) Quantification of Alcian blue positive cells per crypt-villus unit.

(I) Immunofluorescent staining for lysozyme (red), E-cad (green), and DAPI (blue).

(J) Alkaline phosphatase (AP) staining showed representative AP+ inclusion bodies in KO IECs.

(K) Quantification of mis-localized Paneth cells.

(L) Quantification of AP+ inclusion bodies. Data in G, H, K, and L were quantified from multiple intestinal sections of a total of 3 animals per genotype.

Please also see Suppl. Figure 3 and 4.

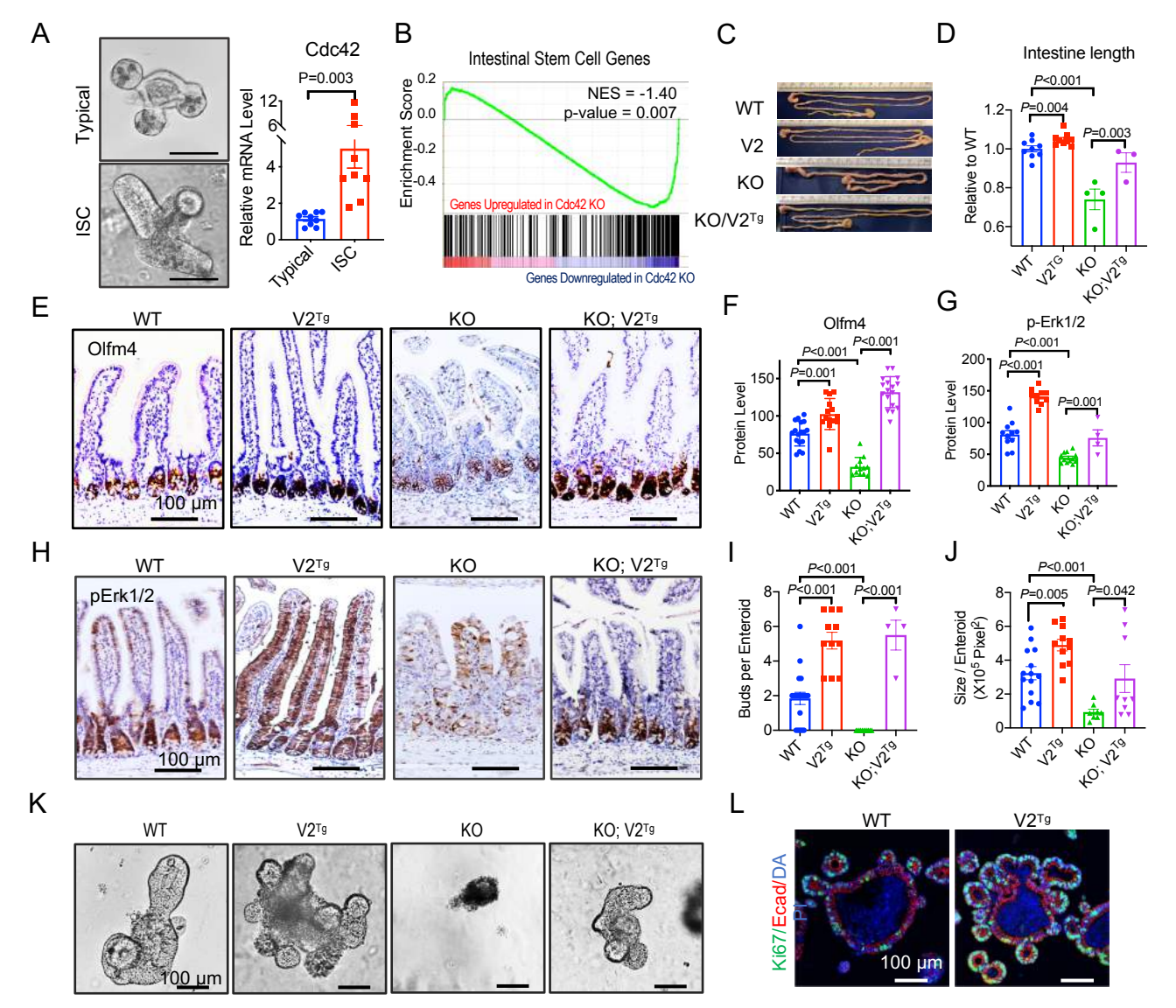
A
Typical
ISC
Cdc42
P=0.003
Relative mRNA Level
Typical
ISC
B
Intestinal Stem Cell Genes
Enrichment Score
NES = -1.40
p-value = 0.007
Genes Upregulated in Cdc42 KO
Genes Downregulated in Cdc42 KO
C
WT
V2
KO
KO/V2Tg
D
Intestine length
Relative to WT
E
WT
V2Tg
KO
KO; V2Tg
Olfm4
100 μm
F
Olfm4
Protein Level
G
p-Erk1/2
Protein Level
H
pErk1/2
100 μm
I
Buds per Enteroid
J
Size / Enteroid (X10^5 Pixel^2)
K
100 μm
L
Ki67/Ecad/DA
100 μm

Figure 5. Overexpressing Cdc42 V2 enhances ISC function and MAPK signaling.

(A) Images of a typical enteroid and an ISC-enriched enteroid induced by CHIR99021 and valproic acid. Quantification RT-PCR for Cdc42 detected higher mRNA level in ISC enteroids.

(B) Gene set enrichment analysis (GSEA) of bulk RNA-seq showed a significantly reduced Lgr5 ISC gene signature (p=0.007) in Cdc42-iKO compared to WT IECs.

(C-D) Representative gross morphology of WT, $V2_{Tg}$, KO and KO; $V2_{Tg}$ mouse intestines. Note $V2_{Tg}$ intestine was noticeably longer than littermate WT.

(E-F) Immunohistochemistry for Olfm4 showed increased crypt base ISCs in $V2_{Tg}$ intestines and decreased in KO intestines. Olfm4 protein level within crypt were quantified from multiple intestinal sections of a total of 3 animals per genotype.

(G-H) Compared to WT mice, pErk1/2$_+$ cells were expanded in $V2_{Tg}$ intestines and became scattered in KO intestines. pErk1/2 protein level within a crypt-villus unit were quantified from multiple intestinal sections of a total of 3 animals per genotype.

(I-J) The average number of epithelial buds per enteroid and the average size of enteroid were quantified from 3 animals per genotype.

(K) Representative enteriods of designated genotypes.

(L) Immunofluorescent staining of enteroid sections showed increased Ki67+ cells in epithelial buds of $V2_{Tg}$ enteroids.

Please also see Suppl. Figure 5.

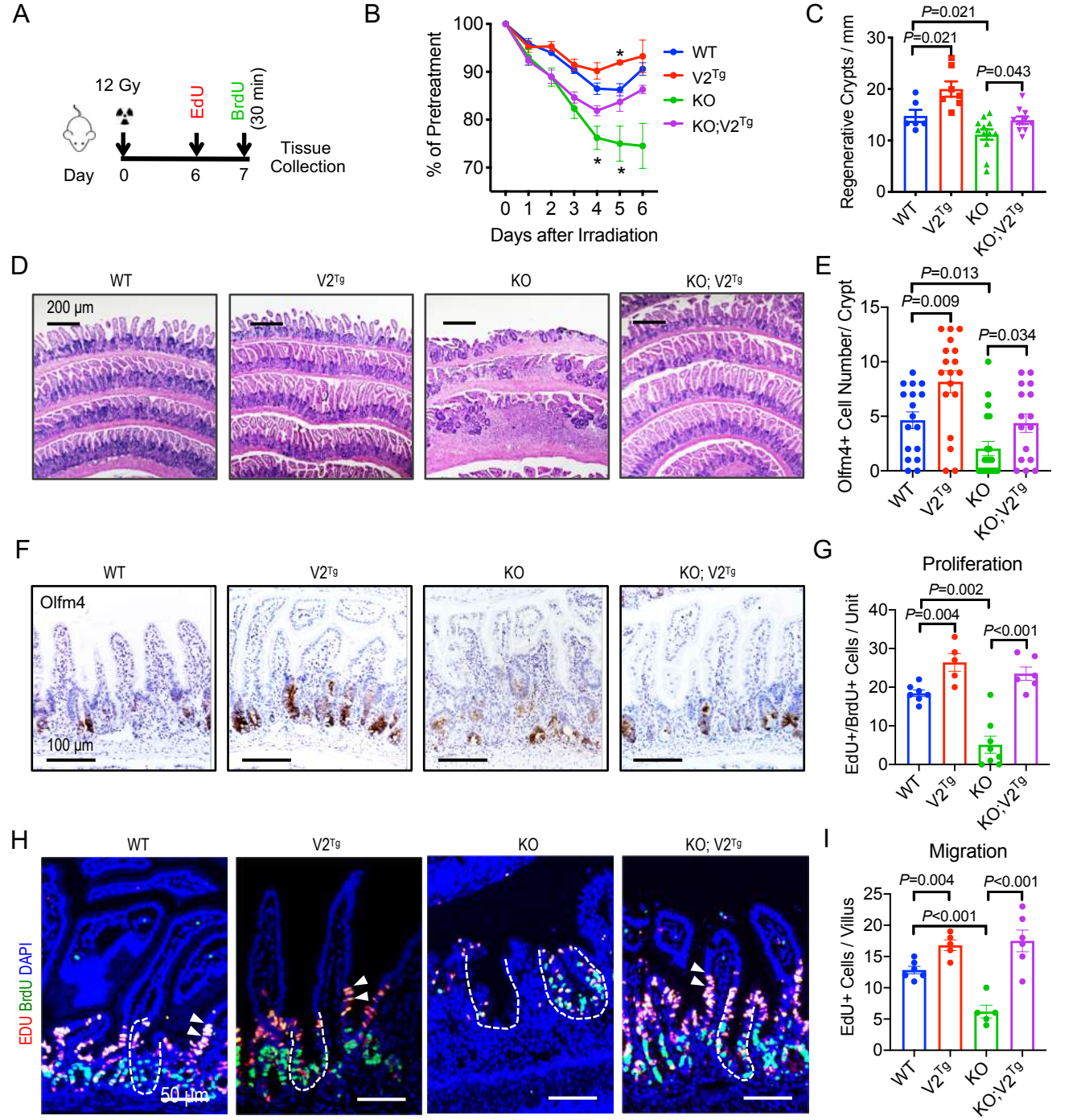
A
12 Gy
EdU
BrdU (30 min)
Tissue Collection
Day 0 6 7
B
% of Pretreatment
Days after Irradiation
WT
V2Tg
KO
KO;V2Tg
C
Regenerative Crypts / mm
P=0.021
P=0.021
P=0.043
D
WT
V2Tg
KO
KO; V2Tg
200 μm
E
Olfm4+ Cell Number/ Crypt
P=0.013
P=0.009
P=0.034
F
Olfm4
100 μm
G
Proliferation
EdU+/BrdU+ Cells / Unit
P=0.002
P=0.004
P<0.001
H
EDU BrdU DAPI
50 μm
I
Migration
EdU+ Cells / Villus
P=0.004
P<0.001
P<0.001

Figure 6. Elevating epithelial Cdc42-MAPK program mitigates mucosal damage following ISC loss.

(A) Mice received a 12-Gy total body irradiation and were sacrificed 7 days after irradiation. Cycling IECs were labeled by sequential injection of EdU (1 day) and BrdU (30 min) before sacrifice.

(B) Percentage of body weight changes were presented as averages of each genotype group (N=8 per genotype). Note there was death of KO animals during the experiment following irradiation. Asterisks indicate $p<0.05$ comparing to WT mice.

(C) Average numbers of regenerative crypts per mm were counted from multiple ileal sections of 3 post-irradiation animals per genotype.

(D) H. & E. stained post-irradiation mouse ileal sections of various genotypes 3 days after irradiation.

(E-F) Number of Olfm4$_+$ cells were counted from immunohistochemistry performed on multiple ileal sections of 3 post-irradiation animals per genotype. Representative images showed Olfm4 staining of different genotypes 3 days after irradiation.

(G-H) EdU (Red) and BrdU (Green) were stained. Average numbers of EdU or/and BrdU labeled IECs per crypt-villus unit were quantified from multiple sections of 3 post-irradiation animals per genotype. Dashed lines indicate crypts; white arrows point to EdU$_+$ and BrdU$_+$ IECs migrating to villi. Nucleus was counterstained with DAPI (Blue).

(I) Average numbers of only EdU-labeled IECs in upper crypt and villus region were quantified from multiple sections of 3 post-irradiation animals per genotype.

Please also see Suppl. Figure 6.

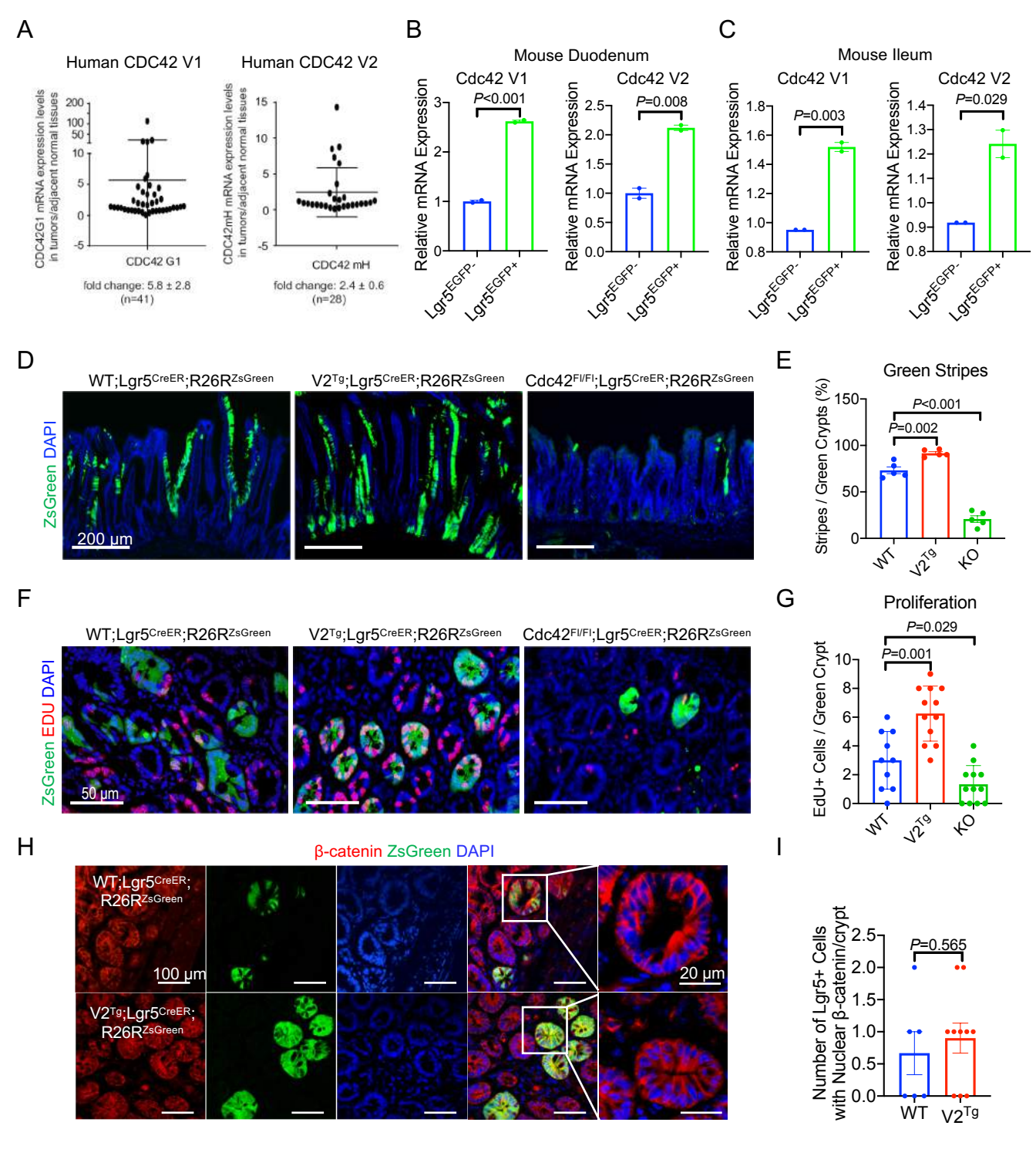
A
Human CDC42 V1
Human CDC42 V2
CDC42G1 mRNA expression levels in tumors/adjacent normal tissues
CDC42 G1
fold change: 5.8 ± 2.8
(n=41)
CDC42mH mRNA expression levels in tumors/adjacent normal tissues
CDC42 mH
fold change: 2.4 ± 0.6
(n=28)
B
Mouse Duodenum
Cdc42 V1
Cdc42 V2
Relative mRNA Expression
P<0.001
P=0.008
Lgr5EGFP-
Lgr5EGFP+
C
Mouse Ileum
Cdc42 V1
Cdc42 V2
P=0.003
P=0.029
D
WT;Lgr5CreER;R26RZsGreen
V2Tg;Lgr5CreER;R26RZsGreen
Cdc42Fl/Fl;Lgr5CreER;R26RZsGreen
ZsGreen DAPI
200 μm
E
Green Stripes
Stripes / Green Crypts (%)
P<0.001
P=0.002
WT
V2Tg
KO
F
WT;Lgr5CreER;R26RZsGreen
V2Tg;Lgr5CreER;R26RZsGreen
Cdc42Fl/Fl;Lgr5CreER;R26RZsGreen
ZsGreen EDU DAPI
50 μm
G
Proliferation
EdU+ Cells / Green Crypt
P=0.029
P=0.001
WT
V2Tg
KO
H
β-catenin ZsGreen DAPI
WT;Lgr5CreER;R26RZsGreen
V2Tg;Lgr5CreER;R26RZsGreen
100 μm
20 μm
I
Number of Lgr5+ Cells with Nuclear β-catenin/crypt
P=0.565
WT
V2Tg

Figure 7. Elevating Cdc42 in ISC promotes injury-induced regeneration.

(A) Taqman real-time PCR for human CDC42 V1 and V2 mRNA were performed on colon tumor tissues and adjacent non-tumor tissues. Data were graphed as ratio of tumor over adjacent tissue. 27 out of 41 tumors showed elevated CDC42 V1 while 12 out of 28 tumors had elevated CDC42 V2.

(B) qPCR for mouse Cdc42 variants was performed on FACS-sorted $Lgr5^{EGFP+}$ versus $Lgr5^{EGFP-}$ IECs from WT mouse duodenums.

(C) qPCR for mouse Cdc42 variants was performed on FACS-sorted $Lgr5^{EGFP+}$ versus $Lgr5^{EGFP-}$ IECs from WT mouse leums.

(D-E) Lineage tracing of Lgr5 ISCs of distinct (*Cdc42-WT, $V2^{Tg}$, or KO*) genotypes 7 days after irradiation using a $R26R^{ZsGreen}$ reporter. EdU was injected 6 hrs before sacrifice to identify cycling ISC descendants. Lineage tracing events were presented as percentage of observed green stripes out of total number of green crypts within the same field. Data represented multiple sections from 2 post-irradiation animals. Note that $V2^{Tg}$ and KO ISCs showed increased and diminished lineage tracing events.

(F-G) The average numbers of EdU^{+} cells per green crypt were quantified from multiple sections of 2 post-irradiation animals.

(H-I) The average numbers of nuclear β-$catenin^{+}$ cells per green crypt were quantified from multiple sections of 2 post-irradiated *$Lgr5^{CreER\text{-}IRES\text{-}EGFP}$; $R26R^{zsGreen}$; Cdc42-WT* and *$Lgr5^{CreER\text{-}IRES\text{-}EGFP}$; $R26R^{zsGreen}$; $V2^{Tg}$* mice.